Investigating the Role of Oncostatin M in Cachexia-associated Muscle Wasting

by

Aylin Domaniku Waraıch

A Dissertation Submitted to the
Graduate School of Sciences and Engineering
in Partial Fulfillment of the Requirements for
the Degree of

Doctor of Philosophy

in

Molecular Biology and Genetics

KOÇ ÜNİVERSİTESİ

July 18, 2024

Investigating the Role of Oncostatin M in Cachexia-associated Muscle Wasting

Koç University

Graduate School of Sciences and Engineering

This is to certify that I have examined this copy of a doctoral dissertation by

Aylin Domaniku Waraıch

and have found that it is complete and satisfactory in all respects, and that any and all revisions required by the final examining committee have been made.

Committee Members:

Assist. Prof. Dr. Serkan Kır

Prof. Dr. Tuğba Bağcı Önder

Prof. Dr. Mehmet Kaya

Assoc. Prof. Dr. Şeref Gül

Assist. Prof. Dr. Şükrü Anıl Doğan

Date:18/07/2024

To my parents who have always been by my side.

ABSTRACT

Cachexia is a devastating syndrome responsible for the death of more than 20% of cancer patients. Cancer-associated cachexia, marked by significant weight loss and fatigue, leads to reduced quality of life and poor survival. Although inflammatory cytokines are identified as the causative agents of muscle atrophy, current anti-cytokine therapies have not successfully attenuated muscle wasting in cancer patients. Through our examination of muscle gene expression, we identified Oncostatin M (OSM) as a strong inducer of muscle atrophy. OSM causes atrophy in primary myotubes through the JAK/STAT3 pathway. RNA sequencing shows that OSM potently induces the expression of atrophy markers and multiple potential atrophy-related genes. Overexpression of OSM by intramuscular adenovirus injection leads to muscle wasting in mice. Muscle-specific deletion of the OSM receptor (OSMR) in tumor-bearing mice rescues the cachexia-driven loss of muscle mass and function. OSM is upregulated in the plasma of cachectic mice; neutralizing circulating OSM helps preserve muscle mass and strength in tumor-bearing mice. OSMR transcripts are elevated in many muscle disorders including Facioscapulohumeral Dystrophy (FSHD) and Duchenne muscular dystrophy (DMD). Taken together, these results suggest that the OSM/OSMR signaling plays a crucial role in inducing muscle atrophy and targeting this pathway may help prevent muscle wasting.

ÖZETÇE

Kaşeksi, kanser hastalarının %20'sinden fazlasının ölümünden sorumlu olan yıkıcı bir sendromdur. Kanserle ilişkili kaşeksi, önemli kilo kaybı ve yorgunluk ile karakterize edilir ve hastaların yaşam kalitesinin ve hayatta kalma oranlarının düşmesine yol açar. İnflamatuar sitokinler kas atrofisi ile ilişkilendirilmiş olmasına rağmen, mevcut anti-sitokin tedavileri kanser hastalarında kas kaybını başarıyla durduramamıştır. Kas dokusu gen ifadesini incelememiz sonucunda, Oncostatin M (OSM)'yi güçlü bir kas atrofisi indükleyicisi olarak belirledik. OSM, JAK/STAT3 yolu üzerinden birincil miyotüplerde atrofiye neden olur. RNA dizilemesi, OSM'nin birçok atrofi ile ilgili genin ifadesini indüklediğini göstermektedir. İntramüsküler adenovirüs enjeksiyonu yoluyla OSM'nin aşırı ifadesi, farelerde kas kaybına yol açarken, OSM reseptörünün (OSMR) tümör taşıyan farelerde kas spesifik olarak silinmesi, kaşeksi kaynaklı kas kütle ve fonksiyon kaybını kurtarmaktadır. OSM, kaşektik farelerin plazmasında artış gösterir; dolaşımdaki OSM'yi nötralize etmek, tümör taşıyan farelerde kas kütlesini ve gücünü korumaya yardımcı olur. OSMR transkriptleri, Fasiyoskapulohumeral Distrofi (FSHD) ve Duchenne musküler distrofisi (DMD) dahil olmak üzere birçok kas bozukluğunda yükselmiştir. Bu sonuçlar bir arada değerlendirildiğinde, OSM/OSMR sinyal yolunun kas atrofisi indüklenmesinde kritik bir rol oynadığını ve bu yolun hedeflenmesinin kas kaybını önlemeye yardımcı olabileceğini öne sürmektedir.

The work presented in this Ph.D. thesis has been published in the following journal articles:

Domaniku-Waraich, *et al.,* Oncostatin M signaling drives cancer-associated skeletal muscle wasting. *Cell reports. Medicine*, 2024. *5*(4), 101498. https://doi.org/10.1016/j.xcrm.2024.101498

Domaniku, A., Bilgic, S. N., & Kir, S. (2023). Muscle wasting: emerging pathways and potential drug targets. *Trends in Pharmacological Sciences.* https://doi.org/https://doi.org/10.1016/j.tips.2023.07.006

Bilgic, S.N. and Domaniku, A. *et al.*, EDA2R-NIK signalling promotes muscle atrophy linked to cancer cachexia. *Nature*, 2023. 617(7962): p. 827-834. https://doi.org/10.1038/s41586-023-06047-y

ACKNOWLEDGMENT

Firstly, I would like to express my deepest gratitude to my advisor, Assist. Prof. Serkan Kır, whose support and guidance have been invaluable throughout the five years of my PhD journey. His kindness, approachability, and unwavering patience as my mentor have made this challenging process very manageable. His commitment to my success has been a constant source of motivation; the insightful feedback and expert advice that he offered have significantly shaped the direction and quality of my research.

I am profoundly grateful to my committee members, Prof. Dr. Tuğba Bağcı Önder and Prof. Dr. Mehmet Kaya, for their time, effort, and constructive suggestions. I am also thankful to the other members of my thesis committee Assist. Prof. Şükrü Anıl Doğan and Assoc. Prof. Şeref Gül, for attending my thesis defense.

I would like to thank the Scientific and Technological Research Council of Turkey (TÜBİTAK) (ARDEB Project no 118Z791; BIDEB Project no 120C128) and the European Molecular Biology Organization (EMBO) for their financial support. I also acknowledge that I was funded by TÜBİTAK BIDEB 2211-National PhD Scholarship Program.

I express my heartfelt gratitude to all my dearest lab mates. Without your support throughout this journey, it would be unbearable to proceed through the difficulty on any day. I would like to especially thank Şevval Nur Bilgiç, my best lab buddy of four years on this journey and one of my dearest friends in life. Thank you for being there in all the highs and lows of this journey. I thank Samet Ağca for his continuous support and great contributions with his statistical skills in every research that we worked on together. Special thanks to Melis Sucuoğlu, Sevgi Döndü Özen, and Dilşad Arabacı for their help to our paper and for their great friendship and positivity. Heartful thanks to Carolin Uslucan, Atakan Özcan and Aleyna Kızılyer for their kind companionship, continuous support and willingness to lend a hand whenever needed. I am deeply grateful for the sense of community and the positive, stimulating environment that you all helped create. Thank you for making this journey not only successful but also truly enjoyable.

To my dear friend Raitha Akkad, your patience and perspective on life have been my source of inspiration. Your insight, wisdom, and companionship have been invaluable. Thank you for your steadfast presence in every step of my life.

To my lovely friend İrem Polat, your support as my first lab buddy from our bachelor's days has been invaluable. From learning everything from scratch to navigating academic pressures together, our bond has transcended the confines of the laboratory. I am deeply grateful for your enduring support and motivation in every aspect.

Finally, I would like to express my deepest gratitude to my family for their unwavering support and encouragement. To my brother, Mert, thank you for your endless love and for always believing in me.

To my husband, Wasay, your understanding and encouragement have been my anchor throughout this journey. Without you, it would be hard to manage the balance between research and family. Thank you for your love, and for always being there for me.

To my parents, the support that you gave me throughout my life is invaluable and unconditional. Your sacrifices and guidance have been the foundation of my achievements. I am endlessly thankful to my mother for her unwavering love, support, and belief in me. This accomplishment would not have been possible without her constant encouragement and sacrifices.

TABLE OF CONTENTS

TABLE OF FIGURES

LIST OF TABLES

ABBREVIATIONS

ActRIIB	Activin A Receptor Type IIb
AIDS	Acquired Immunodeficiency Syndrome
ALS	Amyotrophic Lateral Sclerosis
ATP	Adenosine Triphosphate
BAT	Brown Adipose Tissues
bFGF	Basic Fibroblast Growth Factor
BMD	Becker Muscular Dystrophy
BSA	Bovine Serum Albumin
CASCO	Cachexia Score
CEBPD	CAAT/Enhancer Binding Protein D
CLC	Cardiotrophin-Like Cytokine (CLC)
CNTF	Ciliary Neurotrophic Factor,
COPD	Chronic Obstructive Pulmonary Disease
CSS	Cachexia Staging Score
CT-1	Cardiotrophin-1
DMD	Duchenne Muscular Dystrophy
EDA2R	Ectodysplasin A2 Receptor
EDA-A2	Ectodysplasin A2
EDMD	Emery Dreifuss Muscular Dystrophy
EDTA	Ethylenediaminetetraacetic acid
eIF3-f	Eukaryotic Translation Initiation Factor 3 Subunit F
ELISA	Enzyme-Linked Immunosorbent Assay
FKRP	Fukutin-Related Protein (FKRP)
FSHD	Facioscapulohumeral Dystrophy
GAB1	GRB2-Associated-Binding Protein 1
GDF15	Growth Differentiation Factor 15
GEO	Gene Expression Omnibus

GFRAL	Glial Cell-Derived Neurotrophic Factor Receptor α-Like
HSP	Hereditary Spastic Paraplegia
IgG	Immunoglobulin G
IL-1	Interleukin-1
IL-6	Interleukin-6
JAK-STAT	Janus Kinase-Signal Transducer and Activator of Transcription
JDM	Juvenile Dermatomyositis
JNK	c-Jun N-terminal Kinase
LGMD2A	Limb Girdle Muscular Dystrophy Type 2A
LGMD2B	Limb Girdle Muscular Dystrophy Type 2B
LGMD2I	Limb Girdle Muscular Dystrophy Type 2I
LIF	Leukemia Inducible Factor
LLC	Lewis Lung Carcinoma
MAPK	Mitogen-Activated Protein Kinase
MF20	MyHC antibody
MG132	Proteasome Inhibitor
MRI	Magnetic Resonance Imaging
MuRF1	Muscle-specific RING Finger Protein 1
MyHC	Myosin Heavy Chain
MyoD	Myogenic Differentiation 1
NFKBIA	NFκB Inhibitor alpha
NFKBIE	NFκB Inhibitor epsilon
NFκB	Nuclear Factor-kappa B
NIK	NFκB-inducing kinase
OCT	Optimal Cutting Temperature Compound
OSM	Oncostatin M
OSMR	Oncostatin M Receptor
PDAC	Pancreatic Ductal Adenocarcinoma
PI3K	Phosphoinositide 3-Kinase

PMSF	Phenylmethylsulfonyl Fluoride
RT-qPCR	Reverse Transcriptase- quantitative Polymerase Chain Reaction
SDS-PAGE	Sodium Dodecyl-Sulfate Polyacrylamide Gel Electrophoresis
SEM	Standard Error of The Mean
SHP2	Src Homology 2 (SH2) Domain-Containing Tyrosine Phosphatase 2
SOCS	Suppressor of Cytokine Signaling 3
TA	Tibialis Anterior
TBS-T	Tris-Buffered Saline-Tween20
TGF-β	Transforming Growth Factor-β
TNFα	Tumor Necrosis Factor alpha
UCP1	Uncoupling Protein 1
UPS	Ubiquitin-Proteosome System
WAT	White Adipose Tissues

Chapter 1: INTRODUCTION

1.1 Cachexia syndrome

Cachexia is a devastating metabolic disease characterized by excessive weight reduction, and muscle and adipose tissue loss. The word ‘‘cachexia’’ derives from the Greek words, ‘‘kakos’’ and ‘‘hexis’’ meaning ‘‘the bad condition’’. Cachexia is reported to be one of the main contributors to human morbidity and mortality in the world (Ferrer et al., 2023). The symptoms of cachexia are described as gradual but progressive and often associated with the onset of many disorders, such as aging (i.e., sarcopenia), cancer, chronic obstructive pulmonary disease (COPD), kidney disease, rheumatoid arthritis, AIDS, and immune system complications. Cachexia causes the indirect death of around 20% of cancer patients. Cachectic patients report having poor quality of life (QOL), increased fatigue, low response to anti-cancer therapies, and thus reduced longevity (Argiles et al., 2023; Fearon et al., 2012). Due to its pathophysiological complexity, cachexia leads to an impaired response to chemotherapy (Marceca et al., 2020). There is a lack of potential therapies and an unmet medical need for an effective treatment for cachexia (Dolly et al., 2020).

The exact criteria for defining cachexia are not universally consistent. However, exceeding 5% weight loss within 6 months is accepted as a general criterion. Moreover, a cachexia staging score (CSS) is a questionnaire used to diagnose this syndrome; the weight loss within 6 months, the loss of appetite, the SARC-F questionnaire (consisting of five questions: Strength (S), Assistance walking (A), Rising from a chair (R), Climbing stairs (C), and Falls (F)) for sarcopenia development, the performance status defined by Eastern Cooperative Oncology Group and also several serum markers (such as tumor-secreted markers, skeletal muscle degradation compounds, inflammatory proteins) are controlled to determine the CSS (Argiles et al., 2014; Zhou et al., 2018). To further classify the stage of cachectic patients, a clinically validated method called the cachexia score (CASCO) is used; patients are questioned about the presence of anorexia (an eating disorder leading to severe malnutrition and body weight loss), their performance score, and their QOL (Argiles et al., 2017).

The prevalence of cachexia is shown to vary according to the tumor type; this syndrome is more common in gastric and pancreatic cancer patients (~ 80%), whereas prostate or breast cancer patients suffer less from cachexia-driven weight loss (Figure 1-

1) (Bachmann J., 2008; Baracos et al., 2018). Despite its high prevalence and clinical significance, cachexia remains underrecognized and undertreated in many healthcare settings (Ferrara et al., 2022).

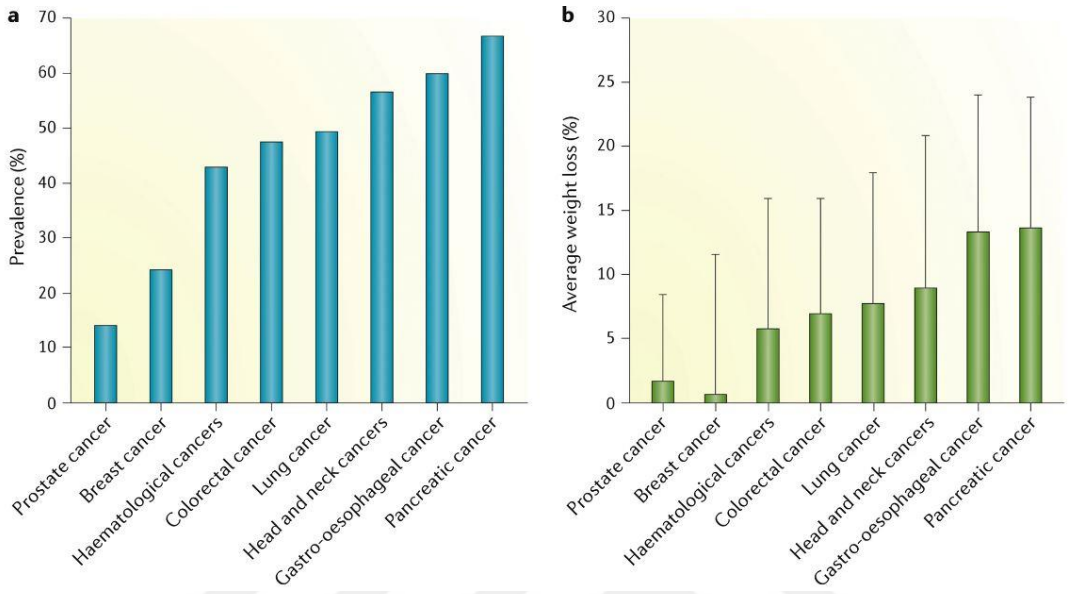

Figure 1-1: The prevalence of cachexia in cancer patients. (A) Prevalence of cancer cachexia and **(B)** its direct association with average weight loss (Adapted from Baracos et al. (2018)).

Cachexia is considered an energy-wasting metabolic disorder. High energy expenditure rather than altered energy intake is the main feature of this syndrome. Several factors affect this imbalance such as tumor type and mass. At the molecular level, the perturbed mitochondria play a huge role in cachexia; activation of uncoupling protein 1 (UCP1) causes the disruption of mitochondrial adenosine triphosphate (ATP) synthesis and is shown to be highly elevated in cachectic conditions in skeletal muscle and in brown adipose tissue (BAT). This is known as mitochondrial uncoupling of oxidative phosphorylation. Moreover, interrupted oxidative fluidity and protein synthesis also cause improper functioning mitochondria in cachexia (Argiles et al., 2014). Another metabolic disturbance is caused in adipose tissues; elevated lipolysis affects the high mobilization of lipid droplets, thus reducing fat mass. Recently, emerging research studies have focused on the relation of cachexia to gut microbiota (Argiles et al., 2023). The gut microbiota, which comprises trillions of microorganisms in the gastrointestinal tract, plays a crucial role in regulating the immune function, nutrient absorption and host metabolism. In cachexia, dysbiosis, defined as an imbalance or disruption in the

composition, diversity, or function of the gut microbiota, is shown to be potentially contributing to systemic inflammation and metabolic dysfunction. Microbial metabolites such as short-chain fatty acids (SCFAs) produced by gut bacteria have been implicated in modulating host energy metabolism and immune responses, which may influence cachexia progression (Bindels et al., 2018).

Due to excessive muscle and fat wasting, cachexia is commonly compared to anorexia. Different from anorexia, despite adequate nutritional intake, cachectic patients continue to lose weight and muscle mass due to metabolic changes associated with their underlying condition (Evans et al., 2008). Understanding the interplay between cachexia and related diseases may help reveal new potential therapeutic targets for managing the progress and the outcome of cachectic patients.

1.2 Skeletal muscle atrophy

Skeletal muscle atrophy, defined as the loss of muscle mass, is characterized by excessive protein catabolism, decreased fiber diameter, and poor muscle strength (Cohen et al., 2015). Muscle wasting is considered a hallmark phenotype of cachexia. This condition is associated with many diseases, primarily with cancer, but also diabetes, organ failures and muscle dystrophies such as Duchenne muscular dystrophy (DMD) and Facioscapulohumeral muscular dystrophy (FSHD) (De Paepe, 2020; Wilkinson et al., 2018). Skeletal muscle is a plastic organ that can adjust its size in response to various conditions such as starvation, immobilization and exercise. Many cytokines and hormones change the balance between protein synthesis and breakdown, the so-called ‘proteostasis’, thus resulting in the re-sizing of muscle fibers and their diameter. An imbalance in proteostasis is often encountered in the conditions of cachexia, aging-related muscle wasting (i.e. sarcopenia) or muscle disuse relatively causing muscle wasting (Furrer & Handschin, 2019).

The excessive protein degradation resulting in muscle atrophy is primarily driven by two of the degradation pathways: the ubiquitin-proteosome system (UPS) and the autophagy-lysosome system (Figure 1-2). The activated UPS is responsible for the reduced muscle contraction and strength. In this proteolytic machinery, the E3 ubiquitin ligase enzymes are responsible for conjugating polyubiquitin tags to proteins tagged for degradation. The muscle-specific E3-ubiquitin ligases Fbxo32 (known as Atrogin1) and

Trim63 (also known as MuRF1, Muscle RING Finger-1) are upregulated during muscle loss (Cohen et al., 2015). Atrogin1 is responsible for the downregulation of protein synthesis mainly by the degradation of myogenic regulatory transcription factor myogenic differentiation 1 (MyoD) and eukaryotic initiation factor 3 subunit f (elF3-f) (Furrer & Handschin, 2019). Atrogin1 also drives the loss of thin filaments (actin, troponins and tropomyosins), actinin and desmin (Sandri, 2013). On the other hand, MuRF1 is responsible for the degradation of proteins functioning in muscle structure, such as myosin heavy chains, myosin light chains 1, actin, myosin-binding protein C, or troponin I. Normally, Atrogin1 and MuRF1 are not necessary for muscle growth; however, blocking either of their expression levels reduces atrophy triggered in different conditions like glucocorticoid treatment, cancer, fasting or denervation (Cohen et al., 2015).

Autophagy is another degradation pathway playing a role in muscle homeostasis (Figure 1-2). This pathway is also activated in response to external stimuli like cellular stress, exercise, or fasting (Aversa et al., 2016). Even though autophagy was once considered a non-selective degradation system, recent studies show that it can degrade specific protein aggregates and also organelles, like mitochondria, via the process called mitophagy (Sandri, 2013). In muscle, misfolded proteins or damaged organelles are engulfed by double-membrane vesicles called autophagosomes. These autophagic cargos are delivered to merge with lysosomes to form autophagolysosomes and get targeted for degradation. The proper balance of the autophagic flux is necessary for maintaining healthy skeletal muscle, and unbalanced autophagy is one of the reasons for pathogenic complications in many muscle diseases (Bonaldo & Sandri, 2013; Sandri, 2013).

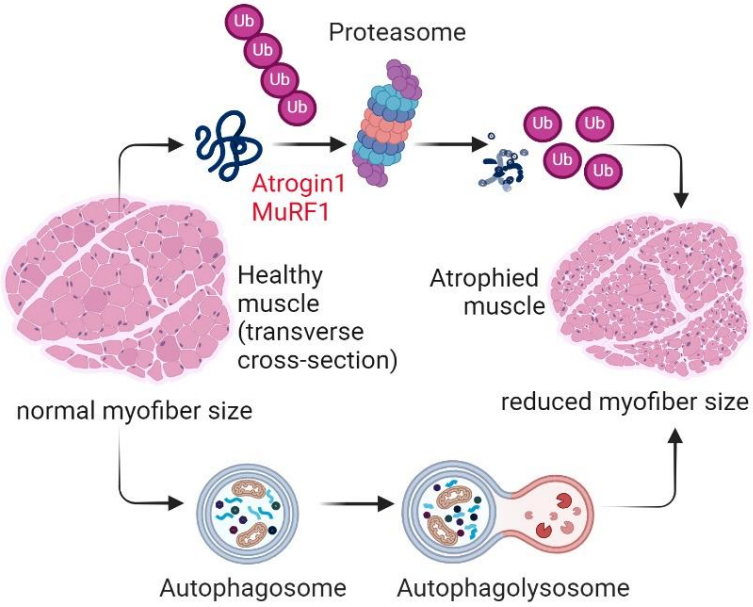

Figure 1-2: The ubiquitin-proteasome system (UPS) and overabundant autophagy promote muscle wasting. The E3 ubiquitin ligases, Atrogin1 and MuRF1, target proteins for degradation in the proteasome. On the other hand, excessive autophagy leads to protein degradation by forming the so-called autophagosomes that evolve into autophagolysosomes. Increased UPS and autophagy causes reduced myofiber size thus leading to muscle wasting (Domaniku et al., 2023).

Identifying the biological conditions and factors triggering cachexia is a major unresolved point that is still elusive in the research field. Recent studies have focused on the effect of inflammation on the catabolic state that underlies cachexia-driven metabolic alterations (Argiles et al., 2023). Tumor secretome induces inflammation, which participates in the general state of cancer-induced cachexia (Baracos et al., 2018). Inflammatory mediators are released from cancer cells or other inflammatory cell types, resulting in muscle weakness, fatigue, and eventually muscle loss (Argiles et al., 2023).

Pro-inflammatory cytokines tumor necrosis factor (TNFα), interleukin-1 (IL-1) and 6 (IL-6) are the known causal agents of cachexia (Webster et al., 2020). TNFα is a cell-signaling protein released by immune cells such as macrophages, neutrophils, mast cells and eosinophils. This protein plays an important role in inducing cell death and immune response. In cachectic cancer patients, TNFα serum levels are elevated. High TNFα levels are related to outcomes of cachexia, such as reduced weight, appetite loss but also increased thermogenesis and increased protein breakdown, leading to induced

muscle loss (Patel & Patel, 2017). However, the clinical studies conducted using TNFα antibodies or inhibitors showed no positive results in cachectic patients (Jatoi et al., 2007; Jatoi et al., 2010). Members of the IL-6 cytokine family are potential targets for the treatment of inflammation, autoimmunity and cancer. The cytokine–cytokine receptor complex of the IL-6 cytokine family is targeted with monoclonal antibodies, specific for cytokines or cytokine receptors, and small-molecule inhibitors that regulate the signaling activity or intracellular mechanisms linked to Janus kinase (JAK)-signal transducer and activator of transcription (STAT) signaling (Jones & Jenkins, 2018). IL-1 and IL-6, as interleukin family members, are two known factors associated with cachexia (Argiles et al., 2023). These proteins play an important role in tissue homeostasis, metabolism, hematopoiesis, and immunity (Jones & Jenkins, 2018). High IL-6 expression is observed in both cachectic patients and murine models of cachexia (Eskiler et al., 2019). However, anti-IL-6 antibodies did not have strong anti-cachectic impacts in the clinic (Bayliss et al., 2011).

Certain research focuses on mediators that target the brainstem and trigger cachexia response. Growth differentiation factor 15 (GDF15) is a cellular stress-responsive cytokine shown to induce cachexia. High GDF-15 levels are detected in mice and patients undergoing weight loss as a result of cachexia (Lockhart et al., 2020). Molecular mediators of the transforming growth factor (TGFb) family are also associated with cachexia. Activin A receptor type IIb (ActRIIB) acts as a receptor for cytokines to bind and activate SMAD2 and SMAD3 transcription factors, which induce the expression of muscle atrophy-related genes.

So far, preventing any of these molecules is not capable of reversing cachexia-driven muscle loss in both research and clinical studies (Dolly et al., 2020; Domaniku et al., 2023). Therefore, the research objective of this thesis is to investigate a new cachectic factor and its molecular mechanism leading to muscle atrophy.

1.3 OSM/OSMR signaling

IL-6 family is a group of cytokines consisting of IL-6 itself, IL-11, leukemia inhibitory factor (LIF), Oncostatin M (OSM), ciliary neurotrophic factor (CNTF), cardiotrophin-1 (CT-1) and cardiotrophin-like cytokine (CLC) (Febbraio, 2007). OSM

has an important role in cell division, homeostasis, and cell death. OSM was initially identified with its antiproliferative effect on melanoma cells (Zarling J., 1986). However, the following studies show its multifunctional roles in both physiological and pathological conditions. This cytokine is released by inflammatory cells like macrophages, T cells, monocytes, and dendritic cells. In response to stimuli, the secreted OSM results in an inflammatory response in the cell (Richards, 2013).

All IL-6 family member proteins contain a 4-helical bundle structure with specific motifs for receptor binding (Chollangi et al., 2012). Oncostatin M, similar to other IL-6 family cytokines IL-6 and LIF, exerts its downstream effects by binding to receptor complexes containing the cell signaling molecule gp130, thus making it with a member of gp130 family cytokines (Hermanns, 2015; Richards, 2013). The Oncostatin M gene is located in on chromosome 22q12, only 20 kilobases away from LIF, showing that they evolved by gene duplication; thus, they are both structurally and functionally very similar compared to other IL-6 family members (Chollangi et al., 2012). Oncostatin M recruits gp130 for higher binding affinity to the other part of the receptor, either the LIF receptor (LIFR) or the specific OSMR receptor-beta chain (OSMRβ). The reason is that Oncostatin M possesses BC loops that create steric hindrance for binding to OSMRβ or LIFR at first. Therefore, it primarily binds to gp130 to further recruit the heterodimer receptors (West et al., 2018). Oncostatin M can itself promote OSMR expression. OSMR is widely expressed in various organs. In humans, the gp130/LIFR complex is termed as OSM receptor type I and the OSMRβ/gp130 complex is termed as the OSM receptor type II (Richards, 2013). In murine models, OSM binds to OSMRβ/gp130 but not the mouse LIFR/gp130 complex, meaning that it cannot engage with the LIF receptor.

Due to its pleiotropic effect, OSM plays different roles in various organs (Figure 1-3) (Hermanns, 2015; Richards, 2013). Recent studies show the role of OSM in ameliorating many non-communicable disorders such as cancer, cardiovascular disorders or diabetes. OSM's effect on cardiomyocyte dedifferentiation protects the heart after acute myocardial damage. However, its prolonged expression in chronic cardiac diseases leads to lethality (Hermanns, 2015). OSM protects mice from obesity-induced metabolic disorders (Komori et al., 2015). OSMRβ-knockout mice are indicated as models for studying metabolic disorders; mice deficient in OSMRβ show improved insulin resistance preceding obesity (Komori et al., 2013). Oncostatin M is involved in muscle physiology by regulating muscle metabolism. OSM functions in muscle regeneration by inhibiting

myoblast differentiation and proliferation (Xiao et al., 2011) and participates in muscle repair following aerobic exercise. In fat tissues, OSM/OSMR signaling maintains adipose tissue homeostasis; in obese mice, fat-specific OSMR knockout worsens insulin sensitivity and leads to inflammation (Komori & Morikawa, 2022). Also, the OSM-OSMR axis plays a critical role in maintaining stromal cell activity in different pathological and physiological events (West et al., 2018).

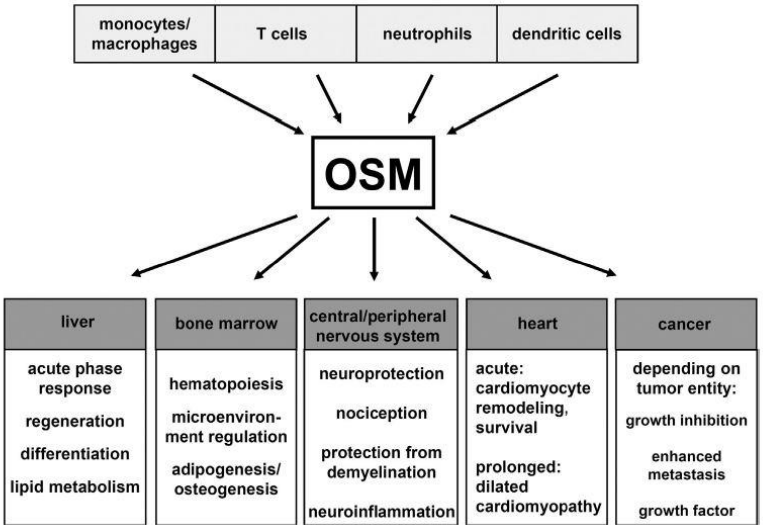

Figure 1-3: The pleiotropic effect of OSM. Oncostatin M plays different roles in tissue and expression-dependent manner (Adapted from Hermanns (2015)).

1.4 JAK/STAT3 signaling pathway

IL-6 family members are known to induce their effects by activating downstream of the Janus kinase/signal transducer and activator of transcription (JAK/STAT) signaling (Babon et al., 2014). The JAK/STAT signaling plays an important role in mediating various processes like cancer, inflammation, hematopoiesis, and tissue repair; deficiency in this signaling is also associated with many autoimmune and metabolic diseases (Dodington et al., 2018). The function of more than 50 cytokines (hormones, interleukins (ILs), interferons (Ifs), and growth factors) are linked to this pathway.

This cascade is composed of ligand-receptor complexes, JAKs, and STATs. There are 4 members of the JAK family: JAK1, JAK2, JAK3, and TYK2. These kinases mediate tyrosine phosphorylation and recruit STAT proteins. On the other hand, the STAT family includes seven members: STAT1, STAT2, STAT3, STAT4, STAT5a, STAT5b, and STAT6 (Hu et al., 2021; Jaskiewicz et al., 2020). JAKs are associated with cytokine receptors and

enable the autophosphorylation of receptors in their tyrosine sites to recruit STAT molecules (Figure 1-4). STATs bind via their Src homology 2 (SH2) domain to the phosphorylated receptors, then get activated, homodimerized, and transported from the cytoplasm into the nucleus. Homodimerized STATs act as transcription factors and bind to DNA to induce the expression of certain genes (Hu et al., 2021).

OSMR/gp130 heterodimers are known to activate JAK1 and JAK2 kinases to further activate STAT1, STAT3 and STAT5 proteins (West et al., 2018). OSM signal attenuation depends on induction of SOCS3 (suppressor of cytokine signaling 3)(Stross et al., 2006). On the other hand, OSMR/LIFR signaling activates mitogen-activated protein kinase (MAPK) cascade via SH2 domain-containing tyrosine phosphatase-2 (SHP2) domain, Phosphoinositide 3-kinase (PI3K) signaling via GRB2-associated-binding protein 1 (GAB1) domain or the STAT3 signaling via JAK1 kinase activation (which is also further attenuated by SOCS3) (West et al., 2018).

STAT3 is known to play a role in tumor formation. It induces angiogenesis and metastasis, thus leading to tumor progression. Moreover, the tumor microenvironment releases the inflammatory IL-6 molecules which then induce their expression via JAK/STAT pathway activation (Jaskiewicz et al., 2020).

In muscle, STAT3 expression is essential for the development of muscle satellite cells. However, excessive expression of STAT3 leads to muscle wasting via induction of muscle cachexia (Jaskiewicz et al., 2020). JAK/STAT3 cascade activation is involved in cachexia-driven muscle loss (Bonetto et al., 2012). STAT3 mRNA levels are increased in cachectic cancer patients compared to non-cachectic and healthy controls (Eskiler et al., 2019). Tumor-bearing muscle-specific STAT3 knockout show improved muscle weight and strength (Silva et al., 2015).

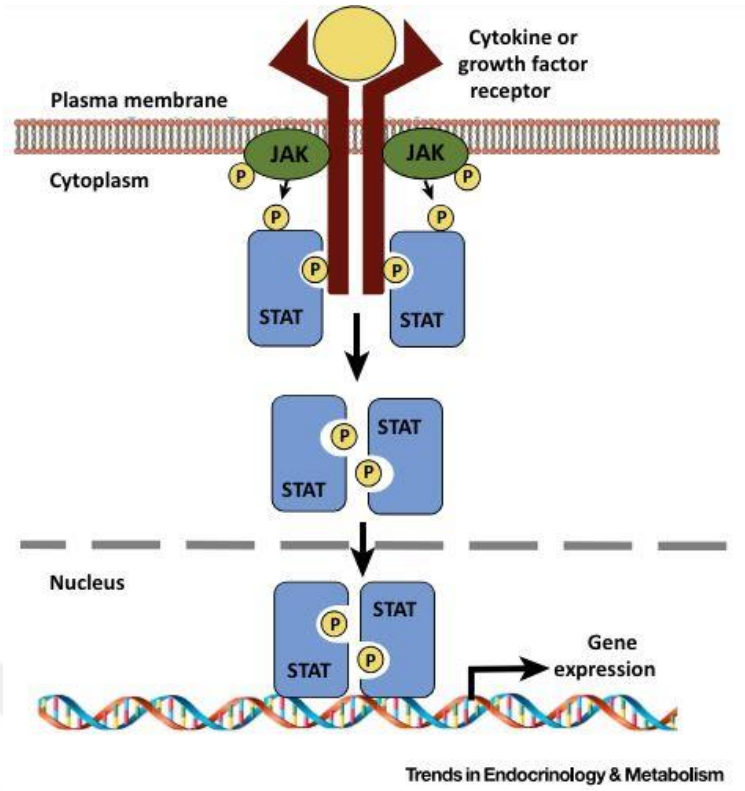

Figure 1-4: The JAK/STAT signaling cascade. Ligands (cytokine or growth factors) bind to their receptor and activate the JAK/STAT pathway. JAK kinases bind to the receptors and auto-phosphorylate to recruit STAT molecules. The activated STAT3 molecules homodimerize and move into the nucleus. They bind to DNA as transcription factors to induce the expression of genes that play a role in cell function (Adapted from Dodington et al. (2018)).

Chapter 2: MATERIALS & METHODS

2.1 Reagents

Mouse recombinant proteins OSM (495-MO), IL-6 (406-ML), and LIF (8878-LF) were obtained from R&D Systems. The JAK1/2 inhibitor Ruxolitinib (Abcam; ab141356) and the proteasome inhibitor MG132 (Sigma; M8699) were obtained from their respective suppliers. The mouse OSM expression plasmid (MR226014) was received from Origene. Prof. Gerhard Müller-Newen (RWTH Aachen University) kindly provided the mouse STAT3-Y705F plasmid. The goat anti-mouse OSM antibody (AF-495-NA) and the control goat IgG antibody (AB-108-C) were purchased from R&D Systems.

2.2 Cell Culture

Mouse primary myoblasts were isolated from the limb muscles of 2-3 day old pups as previously described (Springer et al., 2002). The cells were cultured in Ham's F-10 nutrient mixture (Invitrogen) with 20% FBS (Invitrogen), supplemented with 2.5 ng/mL basic fibroblast growth factor (bFGF) (Sigma) and penicillin/streptomycin (Invitrogen). For differentiation, myoblasts were transferred to DMEM (Sigma 5796) with 5% horse serum and 1% penicillin/streptomycin (Invitrogen). All myotube experiments were repeated at least three times with different batches of myoblast cells, and representative results were reported. Myotubes were harvested 72 hours after the initiation of differentiation in all experiments. Recombinant proteins were administered to the cells for the indicated durations before harvesting. Adeno-GFP was added at the start of differentiation for fluorescent imaging of myotubes using a live cell imager (Zeiss Axiolab live-cell imager). The diameters of individual myotubes were measured using ImageJ software. Treatments with other adenoviruses were conducted 24 hours after differentiation.

2.3 Animal Protocol

All experiments were performed with male mice aged 8-12 weeks. The mice were kept in a 12-hour light/dark cycle (7 a.m. to 7 p.m.) with free access to standard rodent chow and water. The mice were housed in the Koç University Animal Research Facility, and all procedures were carried out following institutional policies and animal care ethics

guidelines. All mice were of a pure C57BL/6 background. Immunodeficient Prkdc^{scid} mice were acquired from Jackson Laboratory (strain #001303). Muscle-specific OSMR-knockout mice were created by crossing OSMR-floxed mice (strain #011081) with ACTA1-Cre mice (strain #006149), both purchased from Jackson Laboratory. Plasma OSM levels were determined using a mouse Oncostatin M (OSM) ELISA Kit (R&D Systems, MSM00). For all tumor inoculation experiments, humane endpoints were defined in accordance with IACUC guidelines. These endpoints included a maximum tumor size of 2 cm (measured as the longest dimension), a body weight loss of 15% or more, and significant lethargy. All animal protocols received approval from the Institutional Animal Care and Use Committee of Koc University.

2.4 Tumor Inoculation

Lewis lung carcinoma (LLC) and B16 (B16-F10) melanoma cells were grown in DMEM medium (Sigma; 5796) containing 10% fetal bovine serum (FBS) and 1% penicillin-streptomycin (Invitrogen). B16 cells additionally received freshly added 2 mM L-glutamine (Invitrogen). During the tumor inoculation experiments, each mouse was housed individually. Five million LLC cells or 2.5 million B16 cells were injected subcutaneously into the flank. Control mice, which did not develop tumors, received only the vehicle (PBS). Sixteen days after LLC inoculation or fourteen days after B16 inoculation, the mice were sacrificed. Epididymal white fat, inguinal white fat, interscapular brown fat, gastrocnemius muscle, tibialis anterior muscle, and tumors were collected and weighed.

2.5 Grip Strength and Inverted Screen Tests

Forelimb grip forces were measured right before sacrifice using a Ugo Basile grip strength meter. For grip strength assessment, each mouse was held by its tail and allowed to grasp a bar connected to a force transducer while being pulled horizontally away from the bar. The peak force applied before releasing the bar was recorded from at least three repetitions and averaged to determine the grip strength of each mouse.

Kondziela's inverted screen test was conducted the day before the sacrifice. Mice were positioned in the center of an inverted wire mesh screen, which was held 60 cm above a cushioned surface. The hanging time was restricted to 1-10 minutes. If a mouse hung for less than a minute, the test was repeated after a resting period.

2.6 Tissue Histology, Immunostaining and Immunohistochemistry

Muscle tissues were snap-frozen in liquid nitrogen-cooled isopentane for 15-20 seconds and then embedded in cryomolds with Tissue-Tek OCT freezing medium (Sakura). Sections of 7 mm thickness were cut using a cryostat (Leica) and placed on Superfrost Plus slides (Thermo). For hematoxylin & eosin staining, sections were fixed with 4% paraformaldehyde and treated sequentially with hematoxylin (Merck 105174), 0.1% HCl, eosin (Merck 109844), a gradient of 70-100% ethanol, and xylene (Isolab). The cross-sectional area of muscle fibers was evaluated using ImageJ software.

For immunostaining, sections were incubated in a blocking solution (3% BSA, 0.1% Triton X-100, and 5% horse serum) for 1 hour at room temperature, followed by overnight incubation at +4°C with primary antibodies (Type IIa fibers, SC-71, DSHB; Type IIb fibers, BF-F3, DSHB; Type IIx fibers, 6H-1, DSHB; Type I fibers, BA-F8, DSHB). After three washes with PBS, sections were incubated for 1 hour in the blocking solution with secondary antibodies (goat anti-mouse IgM H&L Alexa Fluor 488 (ab150121, Abcam) and goat anti-mouse IgG H&L Alexa Fluor 594 (ab150116, Abcam)). Subsequently, sections were washed three times with PBS and mounted using homemade mounting medium before visualization under fluorescence microscopy (Zeiss). The number and cross-sectional area of fiber types were quantified using ImageJ.

For immunohistochemistry, cryosections were cut at 5 μm thickness and fixed with neutral buffer formalin and then incubated with 0.3% hydrogen peroxide for 10 min to block endogenous peroxidase activity. Cryosections were incubated in blocking solution (3% bovine serum albumin + 0.1% Triton X-100 + 5% Horse serum) at room temperature for 1hr and then with anti-OSMR beta (R&D Systems, AF662) antibody (10 μg/ml) in blocking solution overnight at +4°C. Sections were washed with PBS and incubated in the blocking solution containing anti-goat IgG H&L HRP-conjugated secondary antibody (1:1000) (Abcam, ab6885) for 1hr. Finally, the sections were stained with diaminobenzidine (DAB; Abcam, ab64238,) and counterstained with hematoxylin (Merck 105174).

2.7 Adenovirus Production and Injection

Adenovirus vectors were constructed using the Virapower Adenoviral expression system (Invitrogen). The open reading frames of Osm and Stat3-Y705F, preceded by a

CACC sequence, were cloned into a pENTR-D-TOPO plasmid and then recombined into the pAd-CMV-DEST adenoviral plasmid using LR clonase II. The kit provided a LacZ adenoviral plasmid. Following digestion with PacI (Thermo), adenoviral plasmids were transfected into 293A cells using Lipofectamine 2000 (Invitrogen). The 293A cells were cultured in DMEM (Sigma 5796) supplemented with 10% FBS (Invitrogen) and penicillin/streptomycin (Invitrogen). Adenoviral particles were harvested from the cell culture supernatant according to the manufacturer's instructions. Purification and titration were carried out using the Adeno-X Maxi Purification Kit and Adeno-X Rapid Titer Kit from Clontech, respectively.

Mice received unilateral injections of $5x10^8$ infectious units of Adeno-OSM into the TA muscle, while the contralateral muscle received the same dose of control Adeno-LacZ. The mice were sacrificed 7 days later.

2.8 Immunofluorescence

Primary myotubes were fixed with methanol (pre-cooled) at -20°C for 10 minutes, then incubated in a blocking solution (3% bovine serum albumin + 0.1% Triton X-100 + 10% horse serum) for 1 hour at room temperature. Following this, they were incubated with myosin heavy chain (MyHC) antibody (1:1000) (DSHB, MF20) in the blocking solution for 1 hour at room temperature. After washing with PBS, myotubes were incubated with anti-mouse IgG H&L Alexa Fluor 594 secondary antibody (1:2000) (Abcam, ab150116) and DAPI (1:3000) (Cayman, 14285) in the blocking solution for 1 hour at room temperature. Finally, they were mounted using homemade mounting medium and visualized using fluorescence microscopy (Zeiss). The MyHC signal was normalized to the number of myotube nuclei, and fields with a similar density of myotubes were selected for analysis.

2.9 RT-qPCR

Total RNA from cells or tissue samples was isolated using Qiazol reagent (Qiagen) and further purified with RNA spin columns (Ecotech). Tissues were homogenized using the TissueLyzer LT (Qiagen). Subsequently, complementary DNA (cDNA) synthesis was performed using the High-Capacity cDNA Reverse Transcription

kit (Thermo). The resulting cDNA was subjected to RT-qPCR analysis using a CFX Connect instrument (Bio-Rad). Each reaction mixture contained 25 ng of cDNA and 150 nmol of each primer, mixed with iTaq Universal SYBR Green Supermix (Bio-Rad). The ΔΔCt method was used to calculate relative mRNA levels, and these were normalized to β -actin and cyclophilin mRNA. In experiments involving adenovirus injection into TA muscles, Myod served as the internal control. The primers used in the study were as follows:

Table 1: Primers used for qRT-PCR

Gene	Forward (5'-3')	Reverse (5'-3')
Cyclo	GGAGATGGCACAGGAGGAA	GCCCGTAGTGCTTCAGCTT
Actb	TTCTTGGGTATGGAATCCTGTGG	TTTACGGATGTCAACGTCACAC
Myod	CTGCTCTGATGGCATGATGGA	CACTGTAGTAGGCGGTGTCG
Atrogin1	TCAGAGAGGCAGATTCGCAA	GGGTGACCCCATACTGCTCT
MuRF1	TCCTGATGGAAACGCTATGGAG	ATTCGCAGCCTGGAAGATGT
Osmr	TCACAACTCCAGATGCACGC	ACTTCTCCTTCACCCACTGAC
Jak2	CCACCCGTGGAATTTATGCG	TGGCAATCTTCCGTTGCTCT
Socs3	TAGACTTCACGGCTGCCAAC	CGGGGAGCTAGTCCCGAA
Ampd3	CTCCTCTCAGCAACAACAGCC	CTCCATGAGCGCTTCCTTTGTG
Mt1	AGATCTCGGAATGGACCCCA	AGGAGCAGCAGCTCTTCTTG
Mt2	TACTTCCTGCAAGAAAAGCTGC	TGCACTTGTCGGAAGCCTCT
Sln	GGTGGAGAGACTGAGGTCCTT	CCAAGGCTTGTCTTCACTTCCTGA
Serpina3n	AGAGTCTCTCAGGTGGTCC	ACAGTTTCGCAGACATTGGGA
Stat3	AGGAGTCTAACAACGGCAGC	GTCACGATCAAGGAGGCATCA
Igfbp3	ATAAGAAGAAGCAGTGCCGCC	GTCGTCTTTCCCCTTGGTGT
Cebpd3	AGAACCCGCGGCCTTCTAC	ATGTAGGCGCTGAAGTCGAT
Osm	GAACACTGCTCAGTTTGACCC	CGTGAGGTTCGCCTGATTCT
Traf6	CCCAACAGCTCCAATCCCTT	CCAAGTGATTCCTCTGCATCTTT
Ubr2	CATCTTCCTGAGAGTGCGGG	CCCTGGTCGGTCTCTCCATA
Nedd4	TGCTGAACTCTATGGCTCGAA	TTGGCAGCTTATCAGGGGTG
Musa1	CCGGCTAATGAGGGACGTTT	ACTGAATCGCCATACCTTCTCT

2.10 Western Blotting

Total protein from cells was extracted using a lysis buffer comprising 50 mM Tris (pH 7.5), 150 mM NaCl, 1% Triton X-100, 5 mM EDTA, 1 mM PMSF, along with protease inhibitor tablets (Roche) and phosphatase inhibitors (20 mM NaF, 10 mM β-

glycerol phosphate, 10 mM $Na_4P_2O_7$, 2 mM Na_3VO_4). A similar lysis buffer was utilized for tissue samples, with 1% NP40 as the detergent and 10% glycerol added. Tissues were homogenized using a Kinematica (PT1200E) homogenizer, followed by centrifugation at 13,000 rpm for 10 minutes to obtain supernatants as lysates. Protein concentration was determined using the Bio-Rad Protein assay.

For each experiment, 30 mg of protein lysate was separated in SDS-polyacrylamide gel and then transferred onto a nitrocellulose membrane (Thermo). After blocking with 5% non-fat milk in Tris-buffered saline containing 0.05% Tween 20 (TBS-T), the membrane was incubated overnight with primary antibodies in TBS-T containing 5% BSA. The primary antibodies used were obtained from various sources including Cell Signaling Technology (Stat1, phospho-Stat1-Tyr701, Stat3, phospho-Stat3-Tyr705, Stat5, phospho-Stat5-Tyr694, Jak2, phospho-Jak2-Tyr1008, β-actin, p65-RelA, phospho-p65-RelA-Ser536, p105/p50-NFκB, phospho-p105-NFκB-Ser932, p100/p52-NFκB2, IκB, phospho-IκB-Ser32, Ubiquitin), ECM Bioscience (Atrogin1, MURF1), DSHB (MyHC antibody) and R&D Systems (Goat anti-mouse OSM antibody).

Secondary antibody incubation was carried out in TBS-T containing 5% milk, using anti-rabbit or anti-mouse antibodies from Cell Signaling. WesternBright blotting substrates from Advansta were employed to visualize the results on a Chemidoc imaging system (Bio-rad). Blots visualized with a Licor Odyssey CLx imaging system utilized IRDye 680RD anti-mouse and IRDye 800CW anti-rabbit secondary antibodies. The intensity of blot images was quantified using ImageJ Software. Phosphorylated proteins were normalized to their respective total protein signals, while Atrogin1 and MURF1 levels were normalized to β-actin signal.

2.11 Human Gene Expression Analysis

Differential gene expression analysis was performed using GEO2R with default settings. Gene expression profiles from muscle biopsies of non-cancer subjects and cachectic patients with pancreatic ductal adenocarcinoma (PDAC) were retrieved from GEO with the accession number GSE130563 (Judge et al, 2018) and analyzed using GEO2R with default settings. Moreover, gene expression data from skeletal muscle samples of patients with DMD and normal subjects were obtained with the accession number GSE3307 (Dadgar et al,), and differential analysis between DMD and Normal

groups was performed using GEO2R default settings. The gene expression data of the FSHD patients can be found under the accession number GSE140261 (Wong et al., 2020).

Normalized gene expression profiles of skeletal muscle samples from PDAC patients, muscular dystrophy patients, and healthy individuals were obtained from the Gene Expression Omnibus (GEO) database. Microarray datasets (GSE130563, GSE1007, GSE109178, and GSE3307) were analyzed using GEO2R with default settings. RNA sequencing datasets (GSE115650 and GSE140261) were also retrieved from the GEO database. Gene count normalization and fold change calculations were conducted using the DEseq2 R package, as described. p-values were adjusted for multiple testing. Gene set enrichment analysis was carried out using GSEA (v4.1.0) software. In cases where microarray data were provided in multiple files (GSE1007 and GSE3307), they were combined sample-wise to create a unified dataset for GSEA analysis. Analysis of these datasets was performed by Samet Ağca.

2.12 Statistical Analysis

The data are presented as mean ± SEM. Error bars representing SEM in all results were calculated from biological replicates. Two-group comparisons were assessed using a two-tailed, unpaired t-test. Comparisons involving more than two groups were conducted using one-way or two-way ANOVA, with multiple comparisons corrected using Tukey’s post-hoc test.

Chapter 3: RESULTS

3.1 OSMR Expression Is Upregulated in Muscles of Cachectic Mice and Cancer Patients

The Lewis lung carcinoma (LLC) and B16 melanoma are common tumor models used to study cancer cachexia (Das et al., 2011; Kir et al., 2014). Investigating the expression profiles of genes upregulated in muscles of syngeneic LLC and B16 tumor-implanted C57BL/6 mice, we detected high mRNA levels of the *Osmr* together with atrophy markers *Atrogin1* and *MuRF1* (Figure 3-1).

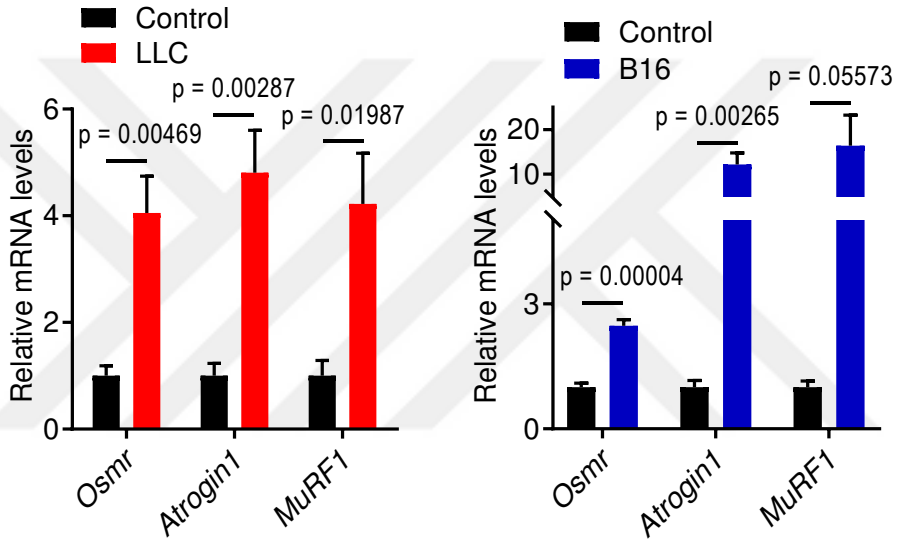

Figure 3-1: Upregulated Osmr mRNA levels in muscles of tumor-bearing cachectic mice. C57BL/6 mice injected with LLC and B16 cells were sacrificed after 16 or 14 days, respectively, and mRNA levels from gastrocnemius muscle were determined by RT-qPCR (n = 5 for the control groups, n = 7 for the LLC group, and n = 5 for the B16 group). The values represent mean ± SEM. Statistical analysis was conducted using the two-tailed t-test.

3.2 OSM Induces Atrophy in Mouse Primary Myoblast Culture

Increased *Osmr* expression in muscles of cachectic mice led us to investigate the effect of OSM in vitro. Primary myoblasts were treated with OSM (250ng/ml) for 48 hours, and the gene expression profile of atrophy markers was analyzed via RT-qPCR. OSM treatment elevated gene expression levels of atrophy marker *Atrogin1* together with *Osmr* in myotubes (Figure 3-2).

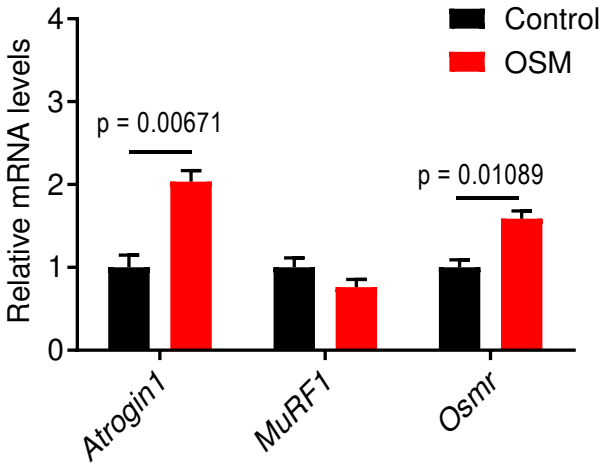

Figure 3-2: OSM induces cellular atrophy. Mouse primary myotubes were treated with recombinant OSM (250 ng/ml) for 48 hr and gene expressions were measured by RT-qPCR (n = 3 for each group). The values represent mean ± SEM. Statistical analysis was conducted using the two-tailed t-test.

To understand if this effect of OSM can drive muscle atrophy, we transduced primary myotubes with GFP adenovirus and treated them for 48 hours with recombinant OSM and other IL-6 cytokine family proteins IL-6 and LIF (250ng/ml all). Cells were visualized under a fluorescent microscope (Figure 3-3A) and myotube diameter was measured (Figure 3-3B). Only OSM promoted drastic shrinkage of myotubes. Moreover, cells were also labeled immunofluorescently via MyHC (Myosin heavy chain) staining (Figure 3-3C); OSM-treated cells showed significantly reduced signal compared to IL-6 and LIF-treated myotubes (Figure 3-3D).

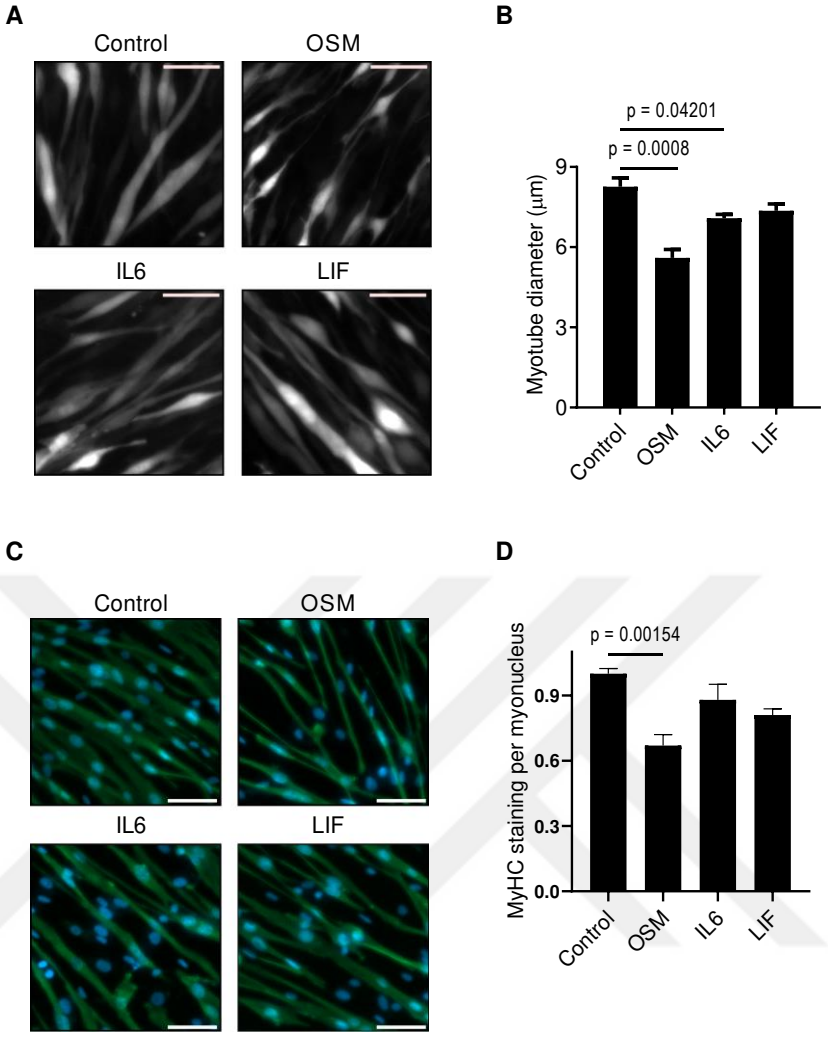

Figure 3-3: Cellular atrophy effect is OSM-specific. **(A)** GFP-transduced primary myotubes were treated with recombinant OSM, IL-6 and LIF (250ng/ml each) for 48hrs and **(B)** their diameter was measured. **(C)** MyHC immunofluorescently labeled cells were treated with OSM, IL-6 and LIF (250ng/ml each) for 48hrs and their nuclei was counterstained with DAPI. The scale bar is 50 µm. **(D)** MyHC signal was quantified and normalized to the number of myotube nuclei (n = 4). Data are presented as mean ± SEM. Statistical analysis was conducted using one-way ANOVA with Tukey's post-hoc test.

To understand the mechanism of OSM-induced cellular atrophy, we tested the levels of MyHC in the presence of MG132, a proteasome inhibitor. The MyHC western blotting shows that in presence of MG132, the reducing MyHC effect is blunted. In fact, OSM treatment in primary myotubes resulted in protein ubiquitination (Figure 3-4A). Moreover, we checked the expression level of E3-ubiquitin ligases; despite *Atrogin1*, OSM-treated primary myotubes induced the expression of also other E3-ubiquitin ligases *Musa1, Traf6, Ubr1* and *Nedd4* (Figure 3-4B). These data conclude that OSM causes atrophy via protein degradation.

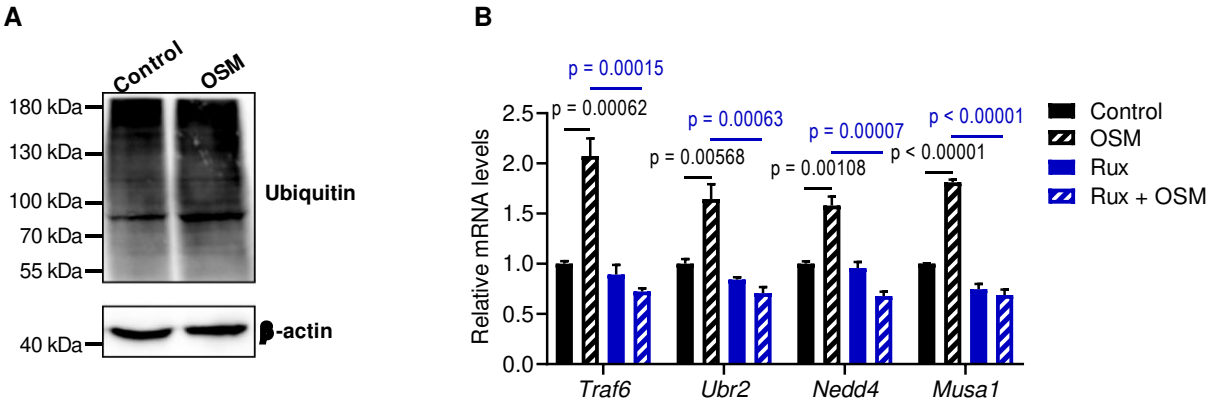

Figure 3-4: OSM induces cellular atrophy via protein degradation. (A) Myotubes were treated with recombinant OSM (250ng/ml, for 48hrs) and MG132 (10mM, for 4hrs); the protein levels were determined via western blotting. **(B)** The cells were treated with OSM (250ng/ml) and Ruxolitinib (2uM) for 48hrs. The mRNA levels were checked via qRT-PCR. Statistical analysis was conducted using 1-way ANOVA with Tukey's post-hoc test.

Furthermore, we analyzed the changes in the gene expression profile of primary myotubes treated with OSM, and IL-6 family members IL-6 and LIF. The RNA samples of these groups were used for RNA sequencing and the results were generated in the form of a heatmap. OSM group showed a distinct expression profile compared to other groups that had comparable patterns in between. The bioinformatics analysis revealed various muscle atrophy-related markers like *Ampd3, Mt1, Mt2, Sln, Cebpd, Igfbp3* and *Serpina3n* to be significantly upregulated in the OSM-treated group compared to the control (Figure 3-5B). The data was validated using qRT-PCR (Figure 3-5A).

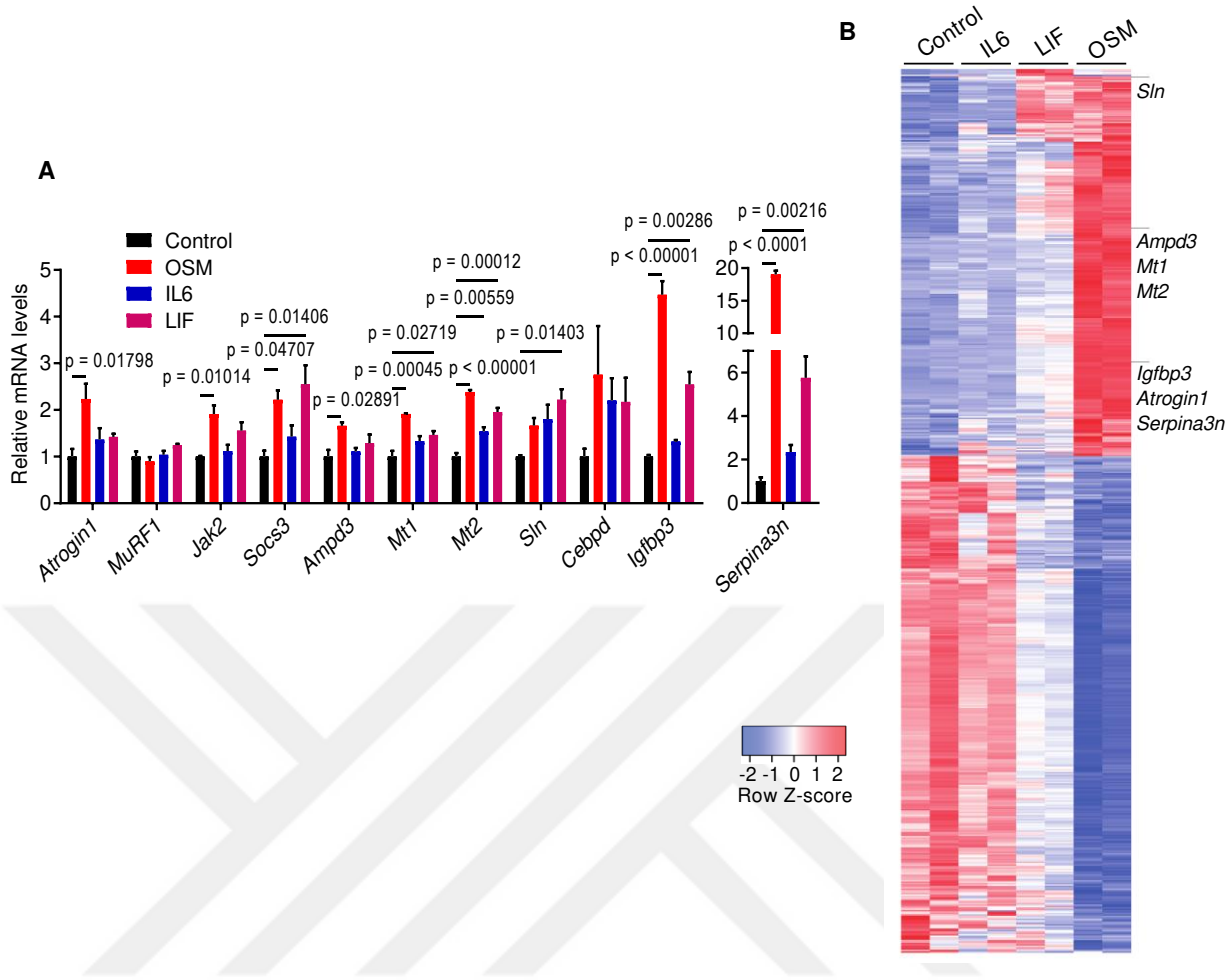

Figure 3-5: The gene expression profiles of myotubes treated with OSM are specific. **(A)** Myotubes were treated with recombinant OSM, IL-6 and LIF (250ng/ml each) for 48hrs. Up-and-down-regulated genes of more than 2-fold were represented in the form of heatmap **(B).** Changes in mRNA levels were checked via qRT-PCR. Data are presented as mean ± SEM. Statistical analysis was conducted using 1-way ANOVA with Tukey's post-hoc test. RNA sequencing analysis was performed by Aynur Kashgari and Samet Ağca.

3.3 OSM Induces Atrophy via JAK/STAT3 Pathway

OSM is known to induce its effects through the JAK/STAT3 pathway and this pathway was previously reported to be activated during muscle atrophy (Bonetto et al., 2012; Richards, 2013). Therefore, we investigated the mechanism of OSM in inducing muscle loss and if this effect occurs via the activation of this cascade. In primary myotubes, we utilized Ruxolitinib (Rux), the JAK2 inhibitor, to block the downstream signaling of the JAK/STAT3 pathway. OSM treatment induced the expression of JAK/STAT pathway components *Jak2* and *Socs3*. Upregulated expressions of *Atrogin1* together with *Osmr* and other OSM target genes were blunted upon treatment of Rux (Figure 3-6). Apart from *Atrogin1*, Rux blunted also the high expression levels of other

E3 ubiquitin ligases *Musa1, Traf6, Ubr1* and *Nedd4* that were upregulated upon OSM treatment (Figure 3-4B). This argues the key role of JAK activation downstream of OSM signaling.

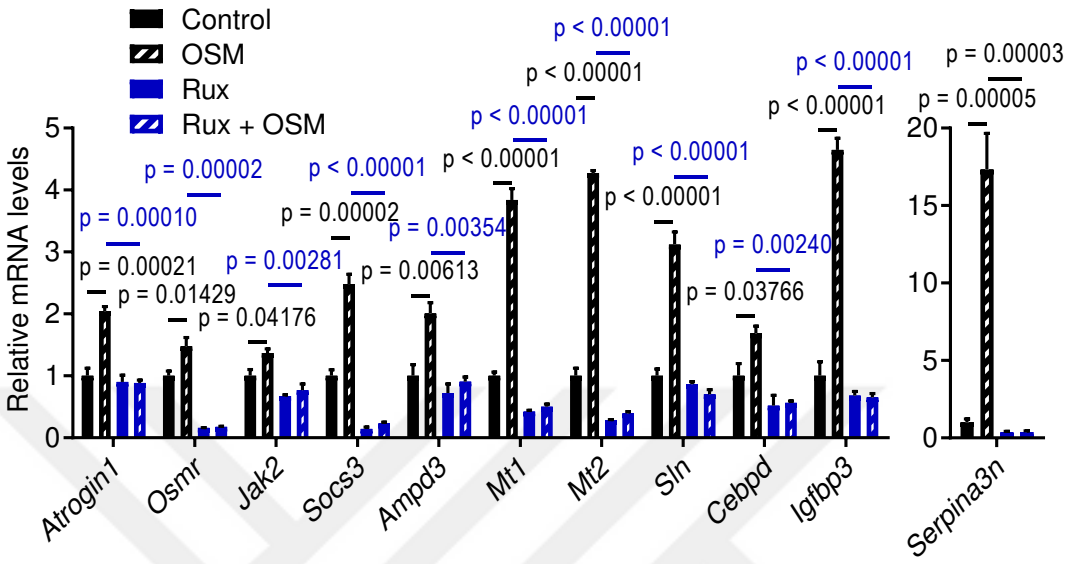

Figure 3-6: OSM induces muscle wasting via JAK/STAT3 pathway activation. Myotubes were treated with recombinant OSM (250ng/ul) and Ruxolitinib (2uM) for 48hrs. Changes in mRNA levels were checked via qRT-PCR. Data are presented as mean ± SEM. Statistical analysis was conducted using 1-way ANOVA with Tukey's post-hoc test.

In addition to mRNA levels, the protein levels were also tested to see the activation of JAK/STAT pathway components. OSM treatment induced the phosphorylation of JAK2, STAT1, STAT3, and STAT5, and their phosphorylation levels were completely blunted via Ruxolitinib treatment (Figure 3-7A). Moreover, to compare if the activation of all the STATs is similar when treated with other IL-6 family proteins, we compared the phosphorylation levels of these proteins also with IL-6 and LIF treatment. Results show that OSM is more potent in inducing the phosphorylation levels of JAK2 and STATs. Equivalent results were obtained also in LIF-treated samples (Figure 3-7B).

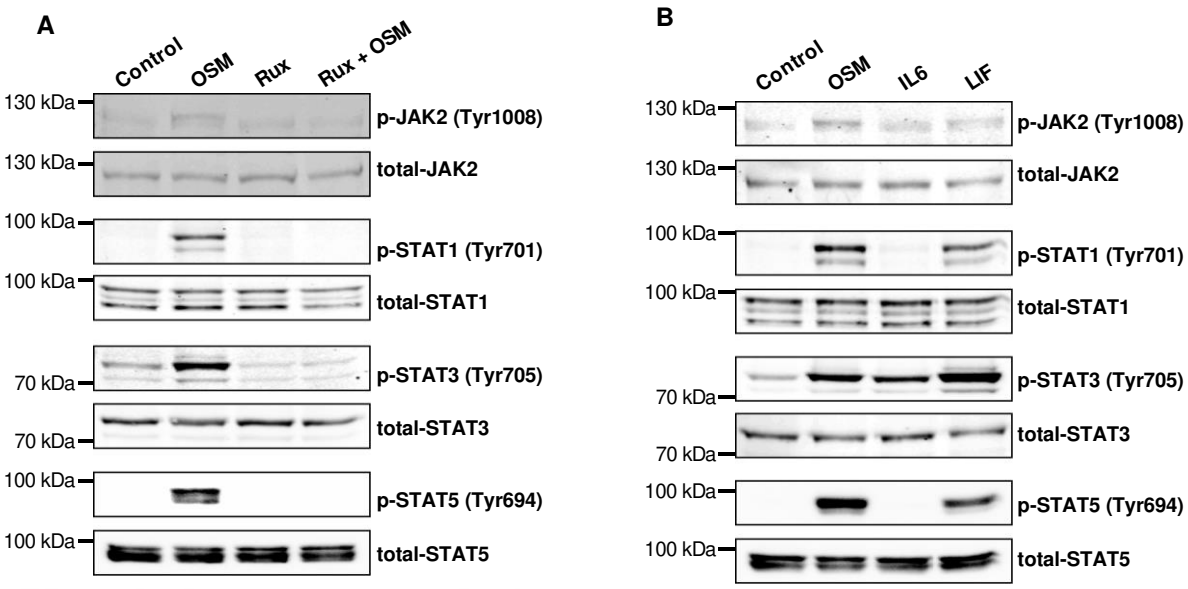

Figure 3-7: OSM induces the protein expression of JAK/STAT3 pathway components (A) Myotubes were treated with recombinant OSM (250ng/ml) and Ruxolitinib (2uM) for 48hrs. **(B)** Cells were treated with recombinant OSM, IL-6 and LIF (250ng/ml each) for 48hrs. Protein levels were determined via western blotting.

To further prove that OSM needs JAK/STAT3 pathway activation to induce atrophy, the primary myotubes were transduced with LacZ and STAT3 mutant (STAT3-Y705F) adenovirus. The STAT3 Y705F has a dominant negative effect that masks the activity of wild-type STAT3. The expression levels of muscle atrophy markers and OSM target genes were analyzed via qRT-PCR (Figure 3-8A). Upregulated mRNA levels of atrophy markers and JAK/STAT3 pathway components upon OSM treatment were blunted in presence of STAT3 mutant adenovirus. The efficiency of STAT3-Y705F was proved via western blotting of STAT3 antibody (Figure 3-8B). OSM-induced phosphorylation of STAT3 was blunted in the presence of STAT3 mutant adenovirus. The blocking effect of STAT3 mutant adenovirus was also observed via imaging (Figure 3-9A). OSM-induced shrinking of myotubes rescued their diameter upon STAT3 blockage (Figure 3-9B). The results point out the need for the JAK/STAT3 pathway to induce cellular atrophy.

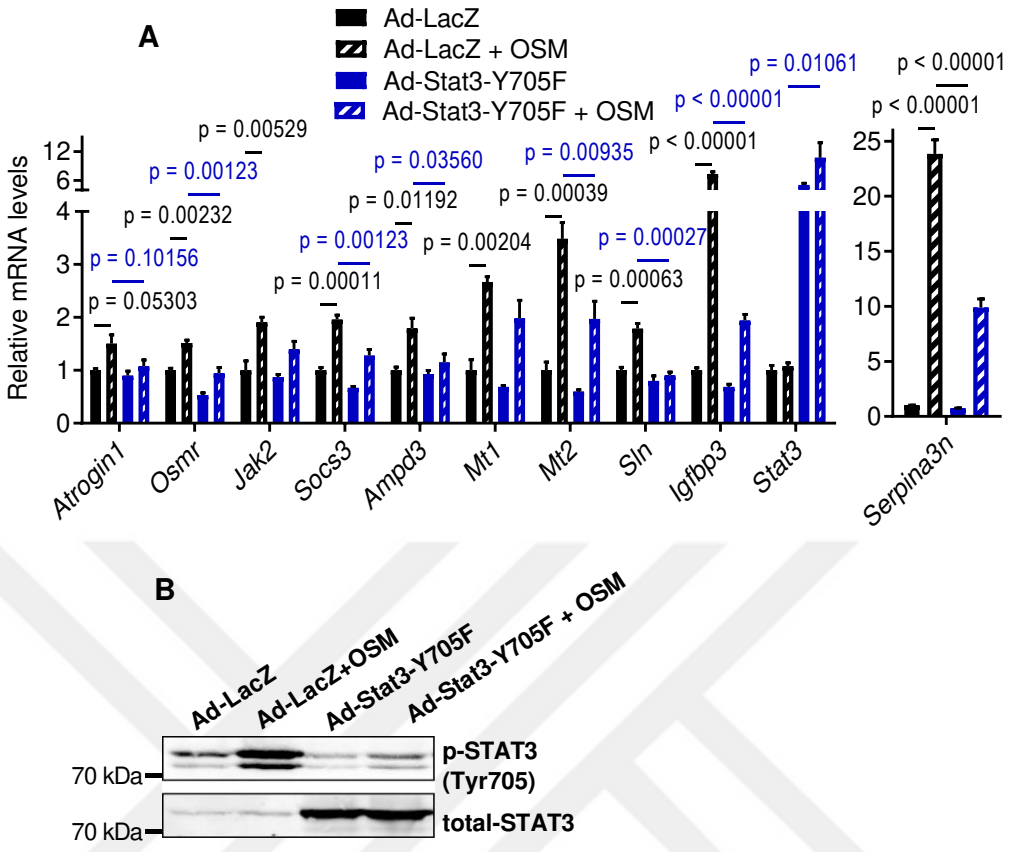

Figure 3-8: Blunted STAT3 activity blocks the atrophy effect of OSM in myotubes. **(A)** Myotubes were transduced with LacZ and Stat3-Y705F expressing adenoviruses and treated with recombinant OSM (250 ng/ml) for 48 h. mRNA levels were determined via qRT-PCR (n = 3). **(B)** Protein levels were determined via western blotting. Data are presented as mean ± SEM. Statistical analysis was conducted using one-way ANOVA with Tukey's post hoc test.

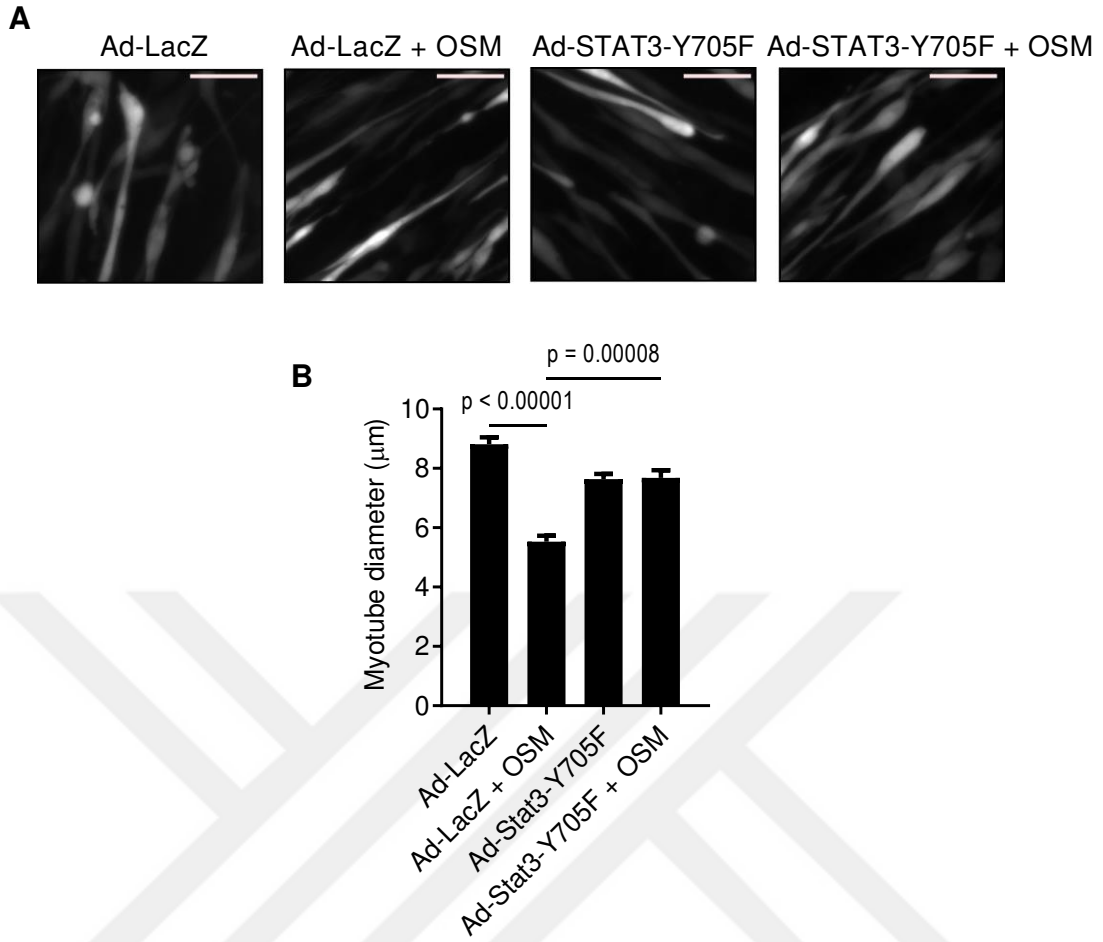

Figure 3-9: Blocking STAT3 activation prevents OSM-induced-cellular atrophy. (A-B) Myotubes were transduced with LacZ and Stat3-Y705F expressing adenoviruses and treated with recombinant OSM (250 ng/mlL) for 48 h. mRNA levels were determined via qRT-PCR (n = 3). The cells were GFP-transduced and visualized. The scale bar is 50um. **(B)** The average diameter of myotubes was measured (n = 4 per group). Data are presented as mean ± SEM. Statistical analysis was conducted using one-way ANOVA with Tukey's post hoc test.

3.4 OSM Overexpression Induces Cellular Atrophy in Primary Myotubes

To determine the effect of OSM on muscle wasting, primary myotubes were transduced with GFP and OSM adenovirus for 48 hours and visualized under microscopy (Figure 3-10A). OSM overexpression significantly reduced the diameter of GFP-transduced cells (Figure 3-10B). Moreover, OSM overexpression also increased the mRNA levels of atrophy markers together with OSM-target genes defined by RNA-seq (Figure 3-10C). Therefore, the data concludes that OSM overexpression in vitro induces cellular atrophy.

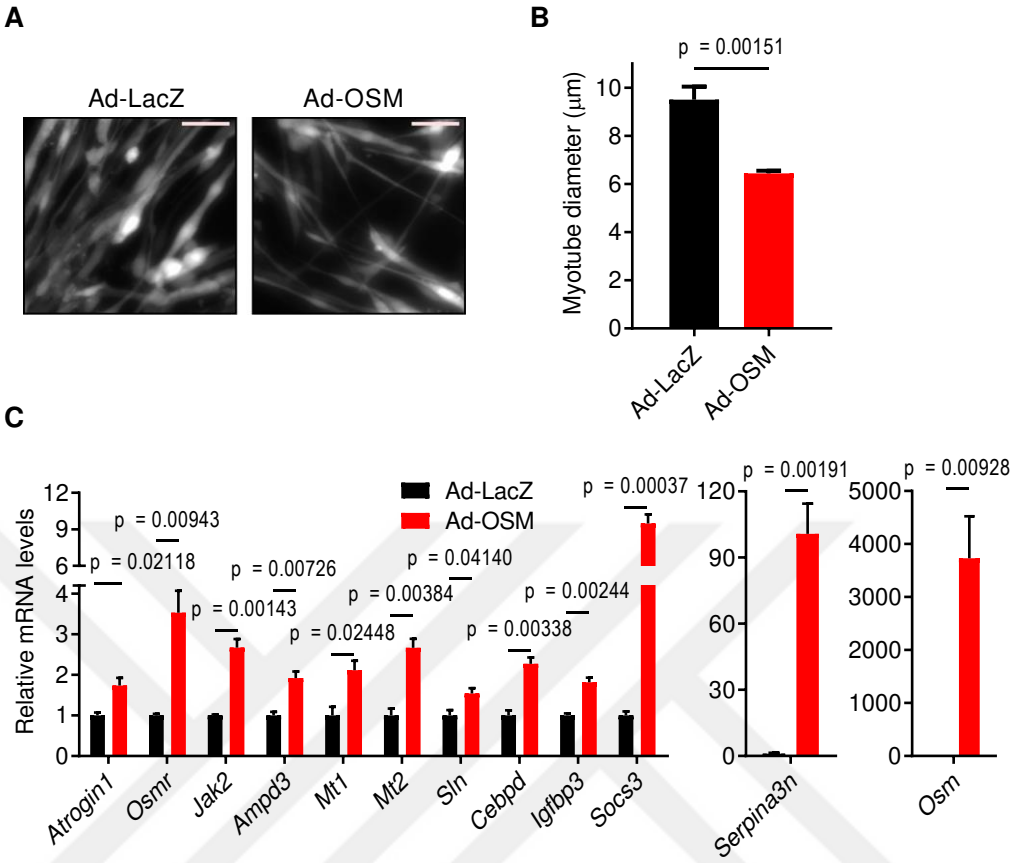

Figure 3-10: OSM overexpression triggers cellular atrophy. **(A)** Myotubes were transduced with GFP, LacZ and OSM-expressing adenoviruses for 48 hrs. **(B)** The average diameter of myotubes was measured (n = 3 per group). The scale bar is 50um. **(C)** mRNA levels were determined via qRT-PCR (n = 3). Data are presented as mean ± SEM. Statistical analysis was conducted via two-tailed t-test. GFP-imaging was performed by Şevval Nur Bilgiç. *Atrogin1, Osmr, Jak2, Osm, Socs3* and *Serpina3n* qRT-PCR were performed by Batu Toledo.

3.5 OSM Overexpression Induces Atrophy *in vivo*

We investigated the atrophy effect of OSM in murine models. We generated adenoviruses and injected intramuscularly into the muscles of mice to overexpress OSM. Seven days after injection, we collected the muscle of mice and H&E stained. The OSM-overexpressed tibialis anterior (TA) muscle had reduced weight, compared to the gastrocnemius muscle, which received no injection (Figure 3-11A). The H&E staining of TA muscle shows that high OSM expression showed significantly reduced fiber area compared to the control group (Figure 3-11B and C). The frequency of small muscle fibers was increased upon OSM overexpression (Figure 3-11D).

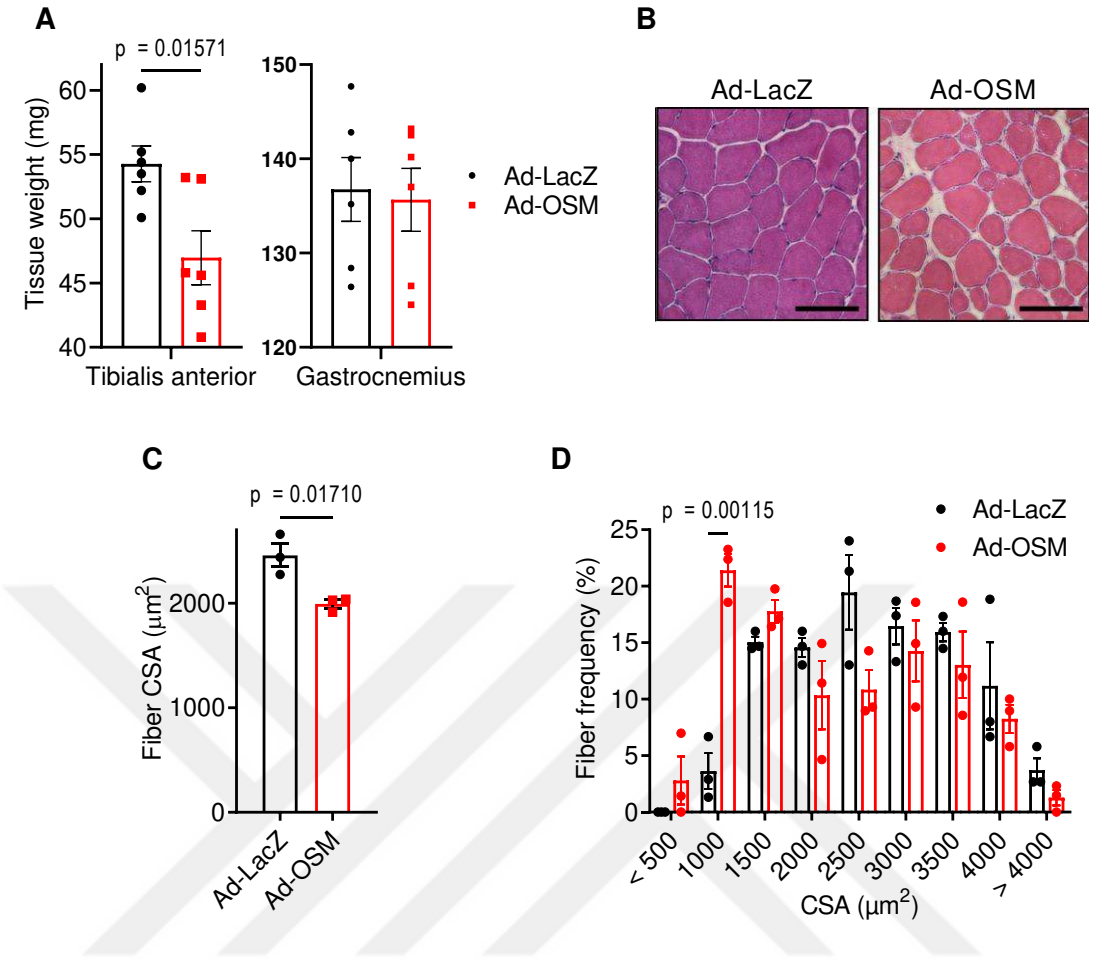

Figure 3-11: OSM overexpression triggers atrophy in muscles of mice. (A) C57/B6 mice were injected with LacZ and OSM overexpressing adenoviruses ($5x10^8$ifu) and sacrificed 7 days later (n = 6 per group). The TA and gastrocnemius muscles were collected and weighed. **(B)** The TA of mice was sectioned, and H&E stained. The scale bar is 100um. **(C)** Muscle fiber cross-sectioned area and **(D)** fiber frequency was measured. Data are presented as mean ± SEM. Statistical analysis was conducted two-tailed t-test. Batu Toledo contributed to tissue weight and collection. Fiber frequency measurements were performed by Samet Ağca.

The mRNA expression levels of atrophy markers, together with JAK/STAT3 pathway components, were upregulated (Figure 3-12). Protein phosphorylation levels of STAT1, STAT3 and STAT5 together with Atrogin1 and MuRF1 were increased in TA of OSM-overexpressed muscles (Figure 3-13A and B). However, only the STAT3 phosphorylation was stimulated by OSM relative to the total protein levels. Overall, the results indicate that OSM induces the expression of muscle atrophy-related genes and activate JAK/STAT3 signaling. These effects results in skeletal muscle wasting in mice.

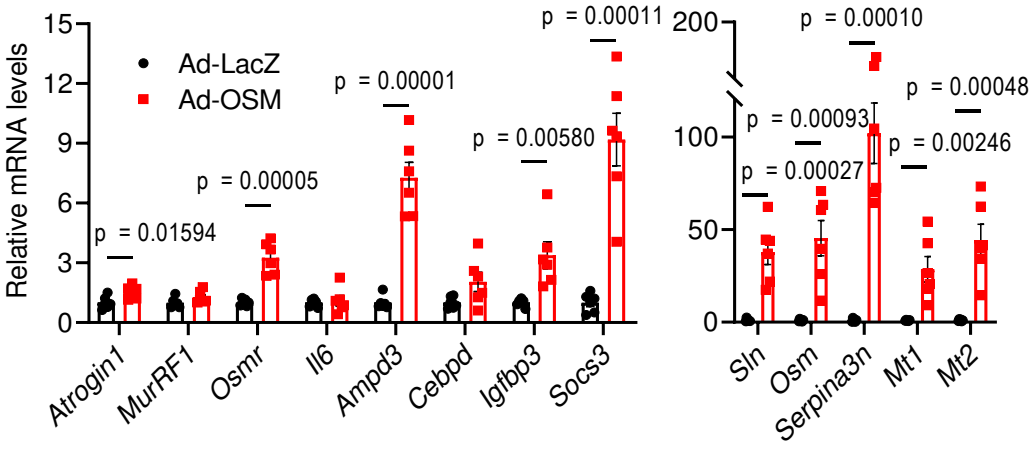

Figure 3-12: OSM overexpression upregulates muscle atrophy markers in vivo. C57/B6 mice were injected with LacZ and OSM overexpressing adenoviruses ($5x10^8$ifu) and sacrificed 7 days later (n = 6 per group). The gene expression levels from TA of mice were determined via qRT-PCR. Data are presented as mean ± SEM. Statistical analysis was conducted two-tailed t-test. The qRT-PCR results were performed by Batu Toledo.

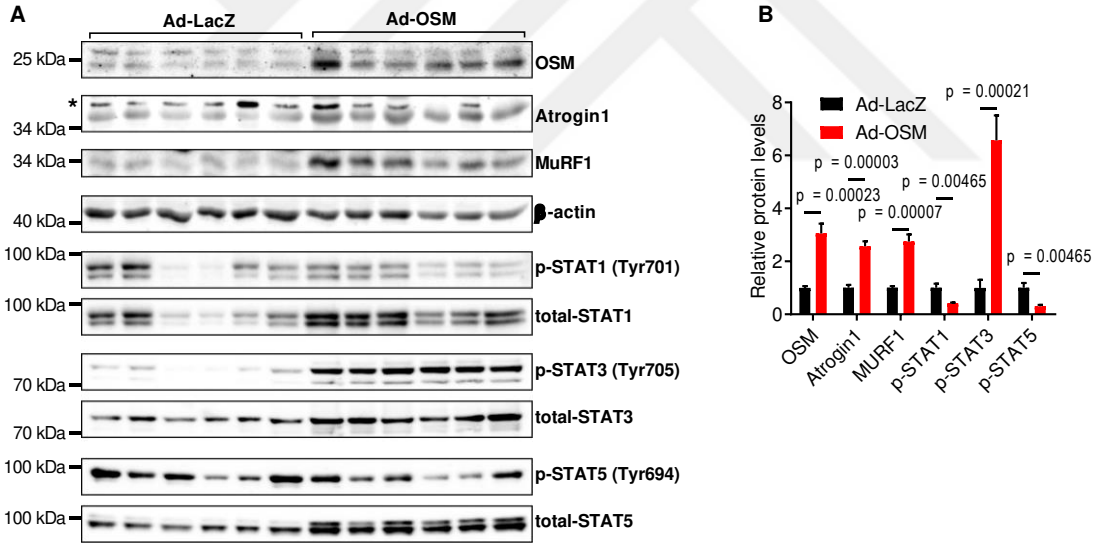

Figure 3-13: OSM overexpression induces the protein expression of JAK/STAT pathway components during muscle atrophy. (A) C57/B6 mice were injected with LacZ and OSM overexpressing adenoviruses ($5x10^8$ifu) and sacrificed 7 days later (n = 6 per group). The protein levels were determined via western blotting and (B) band intensities were quantified. Data are presented as mean ± SEM. Statistical analysis was conducted using two-tailed t-test. Most of the western blotting was performed by Batu Toledo.

We analyzed the effect of OSM in changing in the composition of myofibers upon tumor inoculation. We performed MyHC fiber-type staining on TA muscles. We utilized antibodies staining Type IIa, Type IIb and Type IIx muscle fibers. OSM overexpression

did not change the composition of muscle fiber types, all of which were prone to OSM-induced atrophy (Figure 3-14).

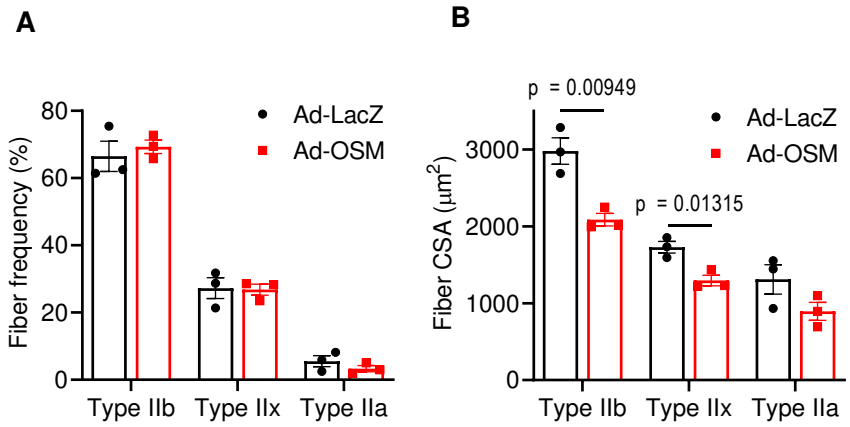

Figure 3-14: OSM overexpression did not affect the fiber-type change in the muscles of mice. (A-B) C57BL/6 mice were transduced with LacZ or OSM-expressing adenoviruses ($5x10^8$ifu) in TA of mice. Mice were sacrificed 7 days after adenovirus transduction (n = 3). Muscle sections were H&E stained and the fiber type frequency **(A)** and cross-sectional area **(B)** were determined by immunostaining (n = 3). Statistical analysis were conducted via t-test. Fiber frequency measurements were performed by Samet Ağca.

3.6 OSM Target Genes are Induced in LLC and B16 Cachectic Mice

We next analyzed the activation of OSM target genes in cachectic models. We inoculated mice with either LLC or B16 and sacrificed 16 days or 14 days later, respectively. In both LLC and B16-inoculated mice, apart from *Atrogin1* and *MuRF1*, OSM target genes that are also considered potential muscle atrophy markers such as were significantly upregulated. In muscles of LLC-bearing mice, the expression levels of *Ampd3, Serpina3n* and *Cebpd* were significantly increased whereas in B16 models, *Mt1, Mt2, Serpina3n* and *Cebpd* mRNA levels were significantly upregulated (Figure 3-15). Phosphorylation levels of JAK/STAT3 components (that are upregulated upon OSM activation) were also analyzed via western blotting. (Figure 3-16A and B). In both cachectic models, among the STATs, only STAT3 phosphorylation was induced. This result argues that STAT3 plays a major role during cachexia. These results prove that OSM and its target genes but also the JAK/STAT3 pathway components are activated in different cachectic models.

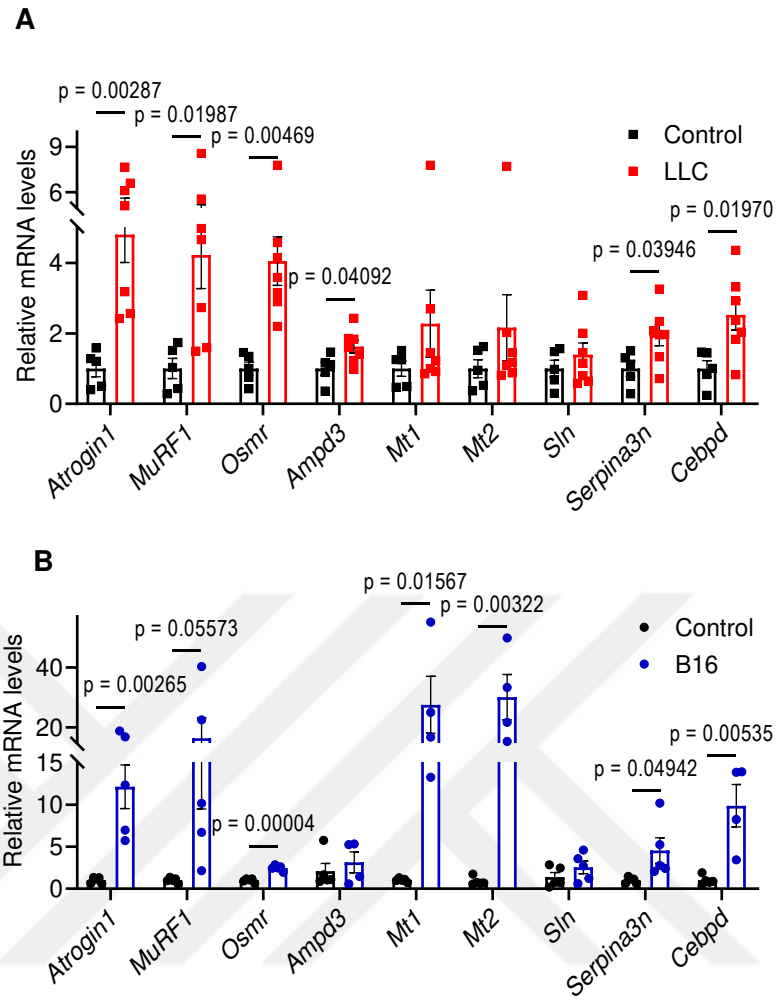

Figure 3-15: OSM overexpression induces the mRNA levels of its target genes. (A) C57/B6 mice were injected with LLC and **(B)** B16 and sacrificed 16 or 14 days later, respectively (n = 6 per group). mRNA levels were determined via qRT-PCR. Data are presented as mean ± SEM. Statistical analysis was conducted using a two-tailed t-test.

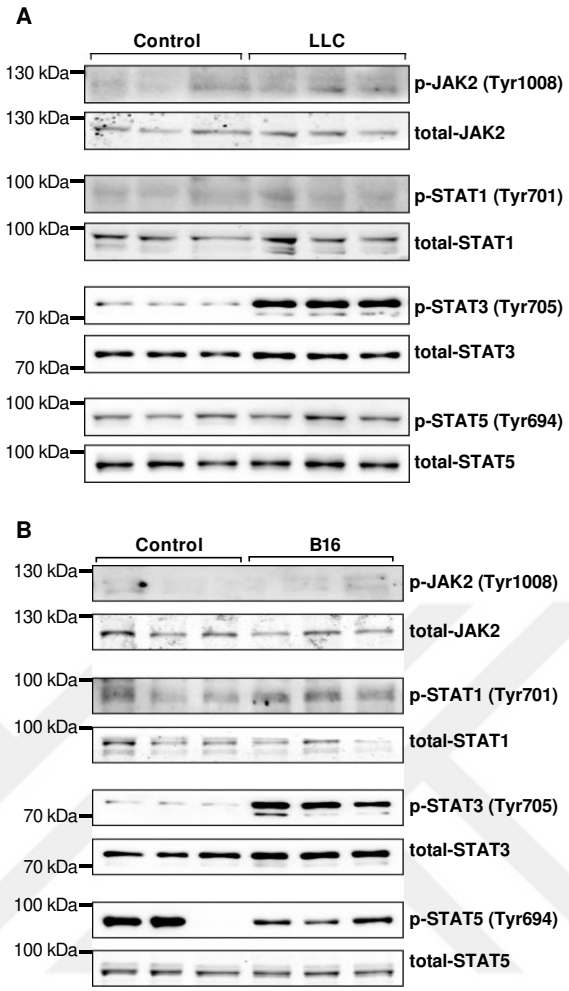

Figure 3-16: OSM overexpression induces the protein expression of JAK/STAT pathway components during muscle atrophy. (A-B) C57/B6 mice were injected with LLC and B16 and sacrificed 16 or 14 days later, respectively (n = 6 per group). The protein expression levels were determined via western blotting.

3.7 Muscle-specific OSMR deletion improves tumor-induced muscle wasting

We next investigated the contribution of the OSM signaling to tumor-induced muscle wasting. We detected high OSM levels in blood plasma of LLC tumor-bearing cachectic mice (Figure 3-17). We generated muscle-specific OSMR knockout (Myo-OSMR-KO) mice. The immunohistochemistry of OSMR expression levels in gastrocnemius muscle confirms its depletion in KO group (Figure 3-19A). We inoculated mice with LLC tumors and sacrificed 16 days later. Grip strength was measured prior to sacrifice. Tumor-induced decrease in gastrocnemius and TA muscle mass of mice was prevented in the Myo-OSMR-KO group (Figure 3-18A). This rescue in muscle mass was significant for TA muscle. Reduced muscle strength in tumor-bearing mice was rescued

in Myo-OSMR-KO mice compared to their wild-type counterparts (Figure 3-18B). Muscles of mice were sectioned and Hematoxylin & Eosin (H&E) stained (Figure 3-19B) and their fiber frequency was measured. The high frequency of fibers with small cross-sectional area (CSA) present in LLC cachectic mice was significantly reduced upon depletion of OSMR (Figure 3-19B and C). Muscle specific depletion of OSMR did not affect tumor-induced wasting of adipose tissues (Figure 3-20).

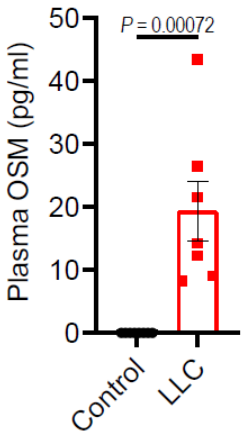

Figure 3-17: Elevated OSM levels are detected in plasma of LLC-bearing cachectic mice. Mice were injected with LLC and sacrificed 16 days later. OSM was measured from their plasma via kit (n = 7 per group).

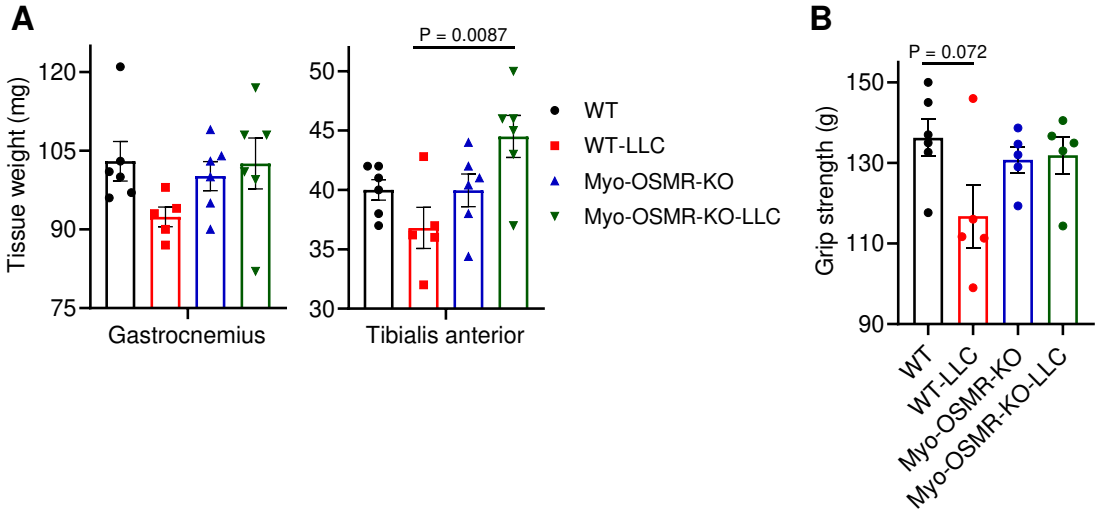

Figure 3-18: Depletion of OSMR protects from LLC-induced muscle loss. (A) Mice were injected with LLC and sacrificed 16 days later (WT-LLC, n = 5 mice; other groups, n = 6). Muscles were collected and weighed. **(B)** Grip strength was measured prior to sacrifice. Data are presented as individual measurements (points) and mean ± SEM. Statistical analysis was conducted using two-way ANOVA with Tukey's post hoc test.

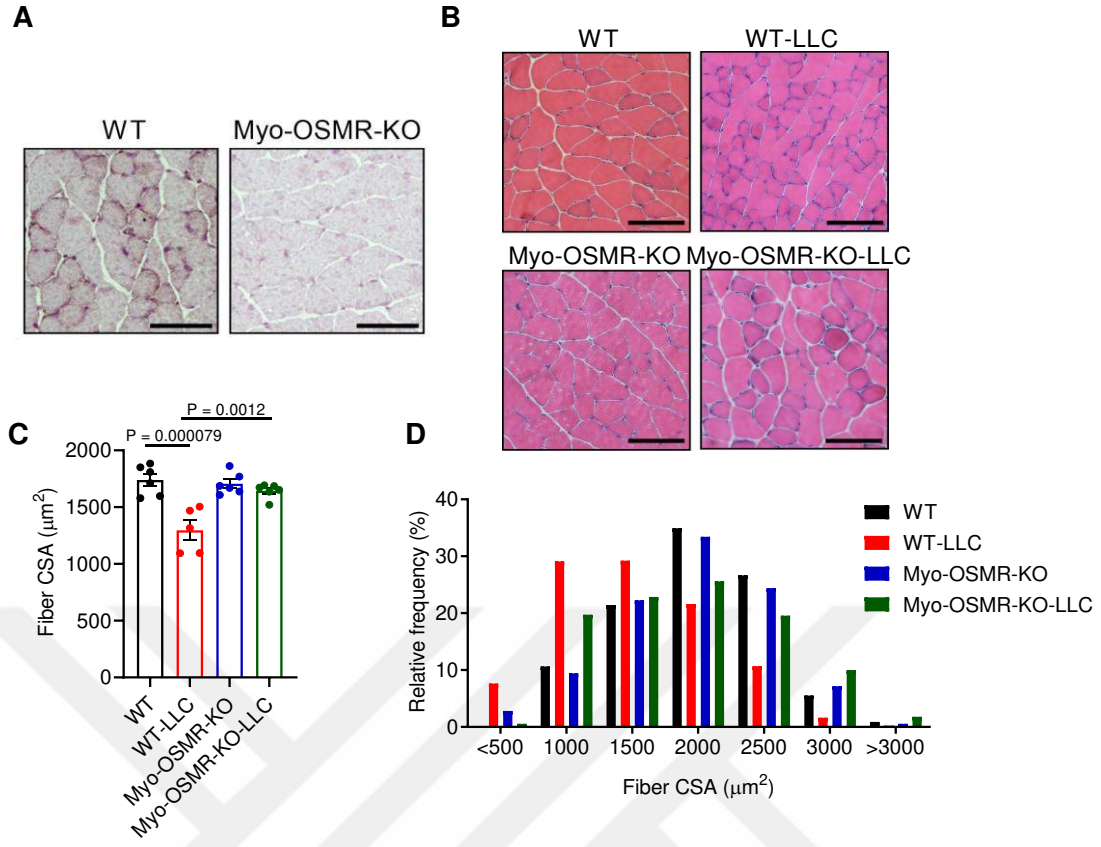

Figure 3-19: OSMR depletion reversed the LLC-driven reduction in myofiber size and frequency. LLC tumor cells were injected to mice and sacrificed 16 days later. **(A)** The immunohistochemistry showing OSMR expression levels in gastrocnemius muscle. **(B)** The muscle tissues were collected, sectioned and H&E stained. **(C)** Fiber cross-sectional area and **(D)** frequency were analyzed. Data are presented as individual measurements (points) and mean ± SEM. Statistical analysis was conducted using one-way ANOVA with Tukey's post hoc test. Fiber frequency measurements were performed by Samet Ağca.

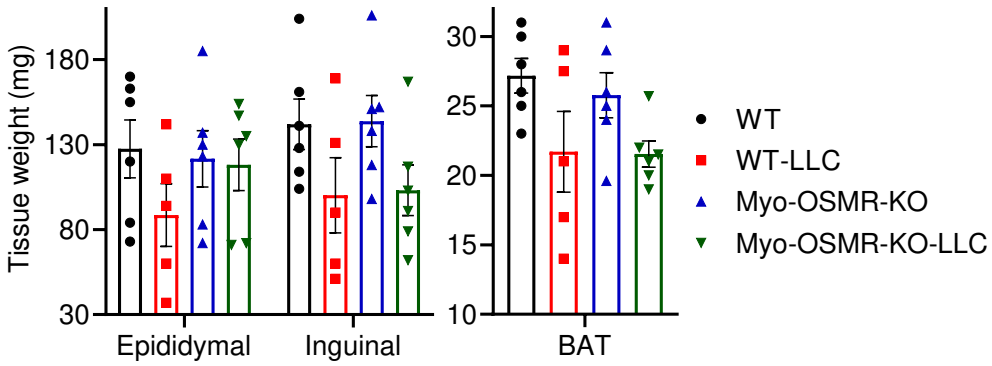

Figure 3-20: Muscle-specific OSMR depletion does not have an effect on adipose tissue wasting. LLC tumor cells were injected to mice and sacrificed 16 days later.

Epididymal, inguinal and BAT tissues were collected and weighed. Data are presented as individual measurements (points) and mean ± SEM. Statistical analysis was conducted using one-way ANOVA with Tukey's post hoc test.

Protein levels of atrophy markers Atrogin1 and MuRF1 are upregulated upon LLC inoculation. However, their expression levels are blunted in Myo-OSMR-KO group (Figure 3-21).

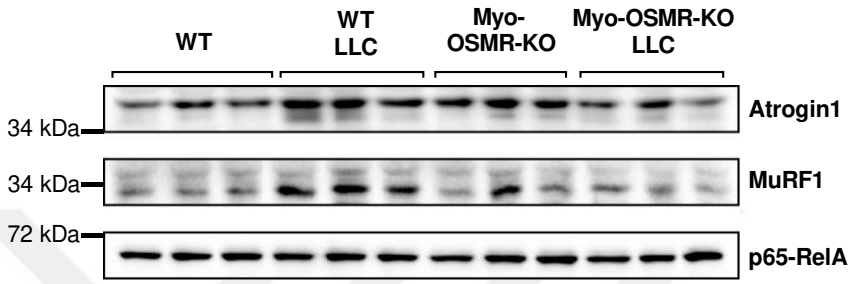

Figure 3-21: High protein levels of atrophy markers got blunted upon OSMR deletion. (A) LLC tumor cells were injected to mice and sacrificed 16 days later. Protein levels were determined via western blotting.

To show that the effect of OSM is not restricted to the LLC cachexia model only, we further inoculated mice with B16 tumors and sacrificed 14 days later. Grip strength and whole limb hanging time, which shows the time mice remain hung in the net with their four limbs, were measured prior to sacrifice. Tumor-induced reduction in muscle mass of mice was rescued in the muscle of Myo-OSMR-KO group (Figure 3-22A). Forelimb grip strength and wholelimb hanging time improved in Myo-OSMR-KO mice compared to their counterparts (Figure 3-22B and C).

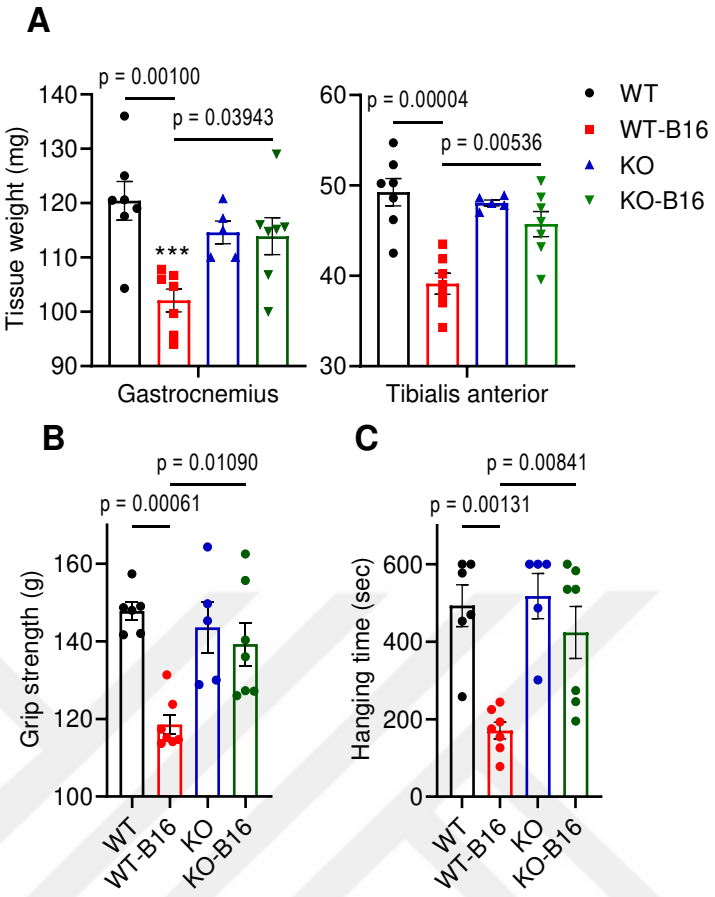

Figure 3-22: OSMR-depleted cachectic mice protect from muscle loss. (A) Mice were injected with B16 and sacrificed 14 days later (n = 6 per group). Muscles were collected and weighed. **(B)** Grip strength and **(C)** hanging time were measured prior to sacrifice. Data are presented as individual measurements (points) and mean ± SEM. Statistical analysis was conducted using 2-way ANOVA with Tukey's post hoc test.

The muscles of B16-inoculated mice were H&E stained, and their fiber frequency was measured (Figure 3-23A). The reduced fiber CSA of muscles in B16 tumor-bearing mice was rescued in Myo-OSMR-KO group (Figure 3-23B). The high frequency of fibers with small CSA present in B16 cachectic mice was significantly reduced upon the depletion of OSMR (Figure 3-23C).

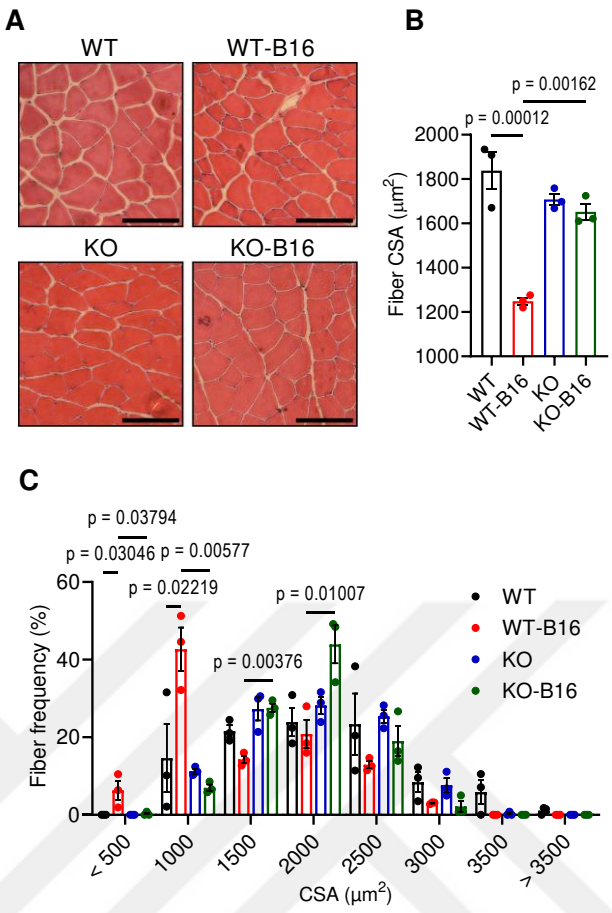

Figure 3-23: Muscle-specific OSMR depletion reversed the B16-driven reduction in fiber size and frequency. (A) B16 tumor cells were injected to mice and sacrificed 14 days later. The muscle tissues were collected, sectioned and H&E stained. **(B)** Fiber cross-sectional area and **(C)** frequency were calculated. Data are presented as individual measurements (points) and mean ± SEM. Statistical analysis was conducted using 1-way ANOVA with Tukey's post hoc test. Fiber frequency measurements were performed by Samet Ağca.

We investigated the fiber type change in muscle of B16 tumor inoculated cachectic mice and OSMR depleted counterpart. There was no significant change in the fiber types upon tumor inoculation. However, there was a slight shift from Type IIb fibers towards Type IIx and Type IIa in Myo-OSMR-KO group (Figure 3-24A and B). Also, the CSA of TypeIIb and Type IIx in B16-inoculated mice was significantly reduced, whereas in B16-MyoOSMR mice, this effect was completely blunted (Figure 3-24C and D).

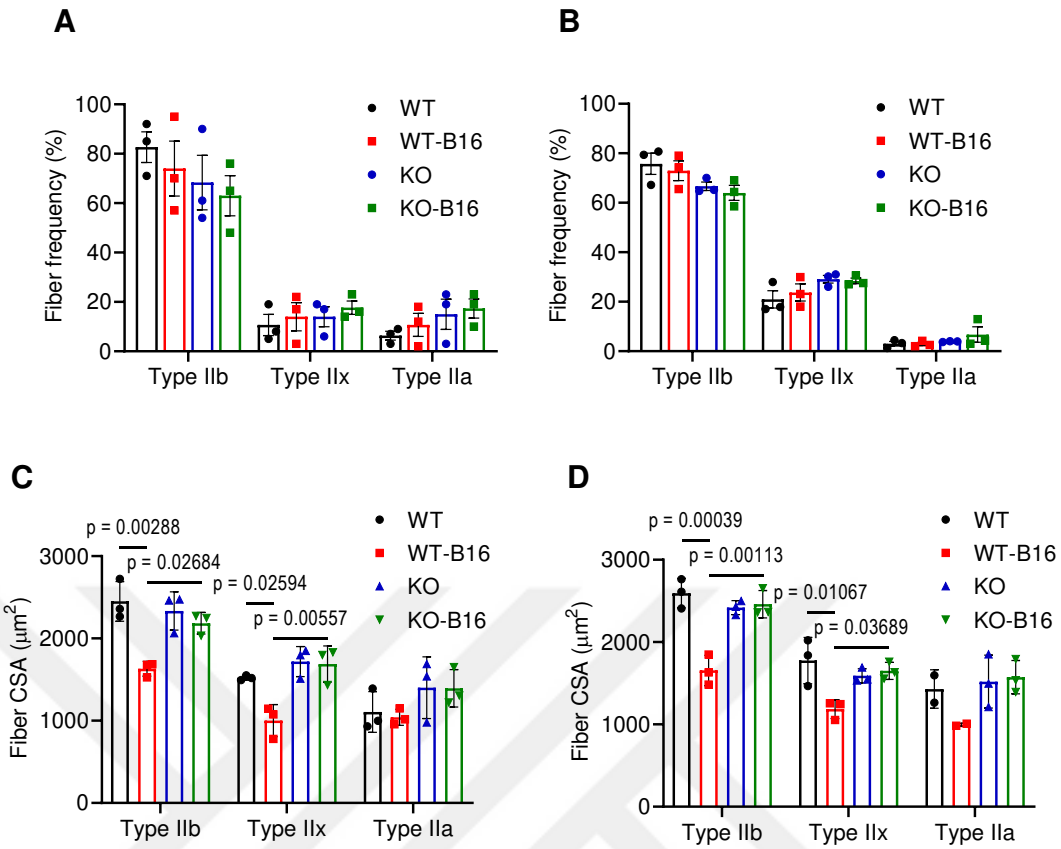

Figure 3-24: Muscle-specific OSMR knockout did not affect the fiber type in mice. (A-B) B16 tumor cells were injected to mice and sacrificed 14 days later. The muscle tissues were collected. Muscle sections were stained, and the fiber type frequency **(A-B)** and cross-sectional area **(C-D)** of gastrocnemius and tibialis anterior muscles, respectively, were determined by immunostaining (n = 3). Statistical analysis were conducted using two-way ANOVA with Tukey's post-hoc test.

High protein levels of atrophy markers Atrogin1 and MURF1 together with STAT3 phosphorylation upon B16 inoculation got blunted in the muscle OSMR deficient mice group (Figure 3-25A and B). Therefore, the results claim that muscle-specific OSMR depletion in mice rescues tumor-induced muscle loss.

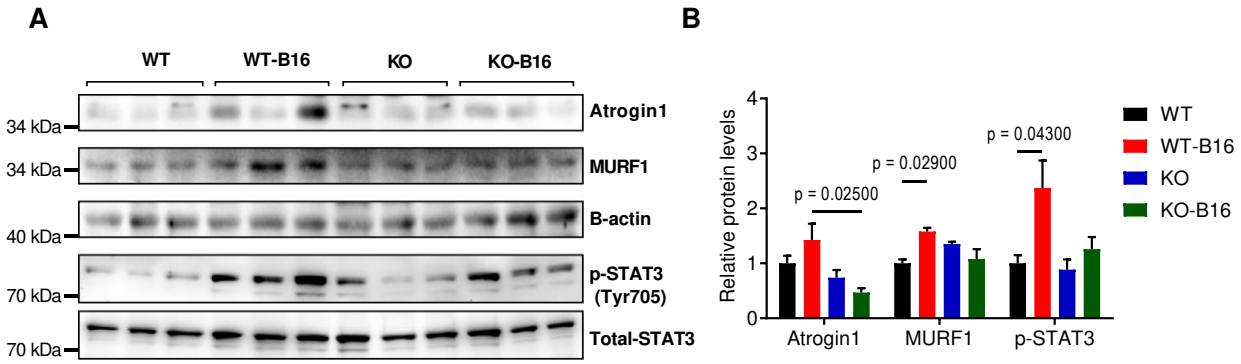

Figure 3-25: High protein levels of atrophy markers are reduced upon OSMR deletion in B16 cachectic mice. (A) Protein levels were determined via western blotting and **(B)** and band intensities were quantified. Statistical analysis was conducted using 1-way ANOVA with Tukey's post hoc test.

3.8 OSM Blockade Ameliorates Muscle Loss in Cachectic Mice

On the therapeutic angle, to test the effect of OSM in cachexia-driven muscle loss, we utilized an OSM-neutralizing antibody. To test the neutralizing effect of the antibody, primary myotubes were treated with recombinant OSM and with IgG and anti-OSM antibodies. The mRNA levels of atrophy markers and OSM-target genes were measured via qRT-PCR. OSM-driven increased atrophy marker gene expression levels, together with the mRNA levels of JAK/STAT3 pathway components, were blunted upon antibody treatment (Figure 3-26).

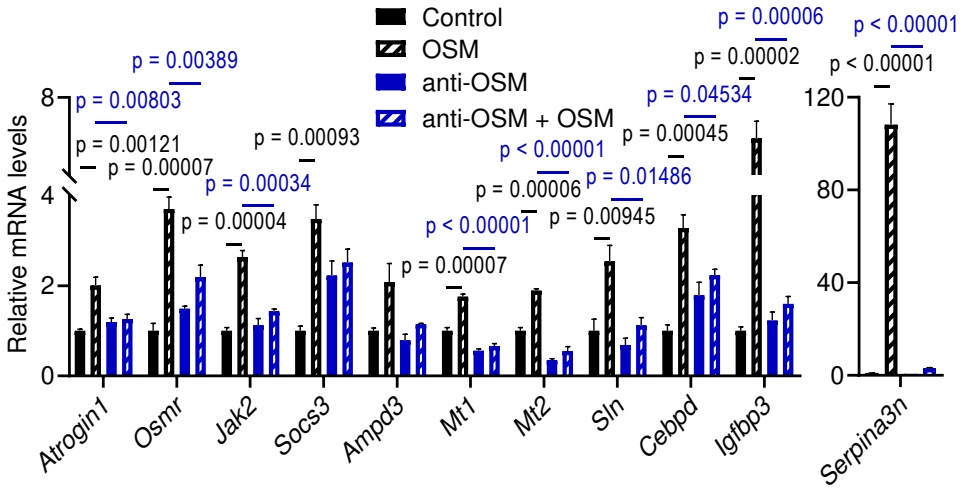

Figure 3-26: OSM blockade rescues cellular atrophy in myotubes. Mouse primary myotubes were treated with recombinant OSM (250 ng/mL) and IgG or anti-OSM antibodies (10 ug/mL) for 48 hrs. mRNA levels were determined by RT-qPCR (n = 3 for

each group). Data are presented as individual measurements (points) and mean ± SEM. Statistical analysis was conducted using 1-way ANOVA with Tukey's post hoc test.

Next, we tested the OSM-neutralizing antibody using the LLC tumor model. We inoculated LLC cells to mice for tumor model generation; then we administered antibody at days 10, 12, 14, and 15 post-tumor injections (Figure 3-27A). On day 16, we measured the grip strength between the groups and sacrificed the mice. Muscle tissues were collected and weighed. OSM-neutralization rescued the reduced muscle weight in tumor-bearing mice (Figure 3-27C). There was no difference in tumor weight between the control and antibody-administered group (Figure 3-27B). The grip strength of mice was partially rescued in antibody treated tumor group compared to its tumor counterpart (Figure 3-27D).

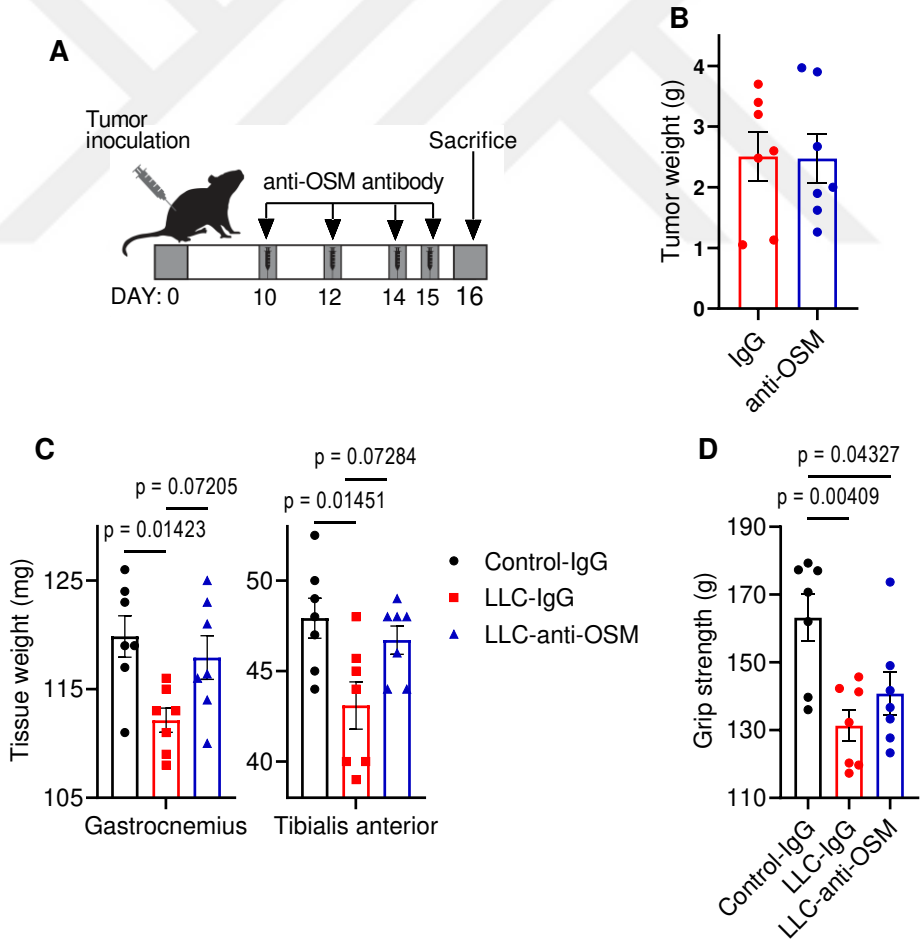

Figure 3-27: OSM neutralization rescues muscle loss in cachectic mice. (A) The setup of antibody treatment; the LLC tumor cells were injected to mice, IgG and anti-OSM antibodies (1mg/kg) were administered at day 10, 12, 14 and 15 post-tumor inoculation.

Mice were sacrificed at day 16. **(B)** Tumors and **(C)** muscle tissues were collected and weighed. **(D)** Grip strength of mice was measured prior to sacrifice. Data are presented as individual measurements (points) and mean ± SEM. Statistical analysis was conducted using 1-way ANOVA with Tukey's post hoc test.

Moreover, the results from H&E-stained gastrocnemius muscle (Figure 3-28A) showed that the fiber cross-sectional area and frequency of fibers with large cross-sectional area in cachectic mice increased OSM neutralization (Figure 3-28B and C). The high protein levels of atrophy markers Atrogin1 and MURF1, together with STAT3 phosphorylation in LLC group were suppressed in antibody-given tumor-bearing counterpart (Figure 3-29A and B). The results demonstrate that OSM/OSMR angle plays a crucial role in cachexia-driven muscle loss, and targeting this signaling pathway can help reverse tumor-induced muscle loss.

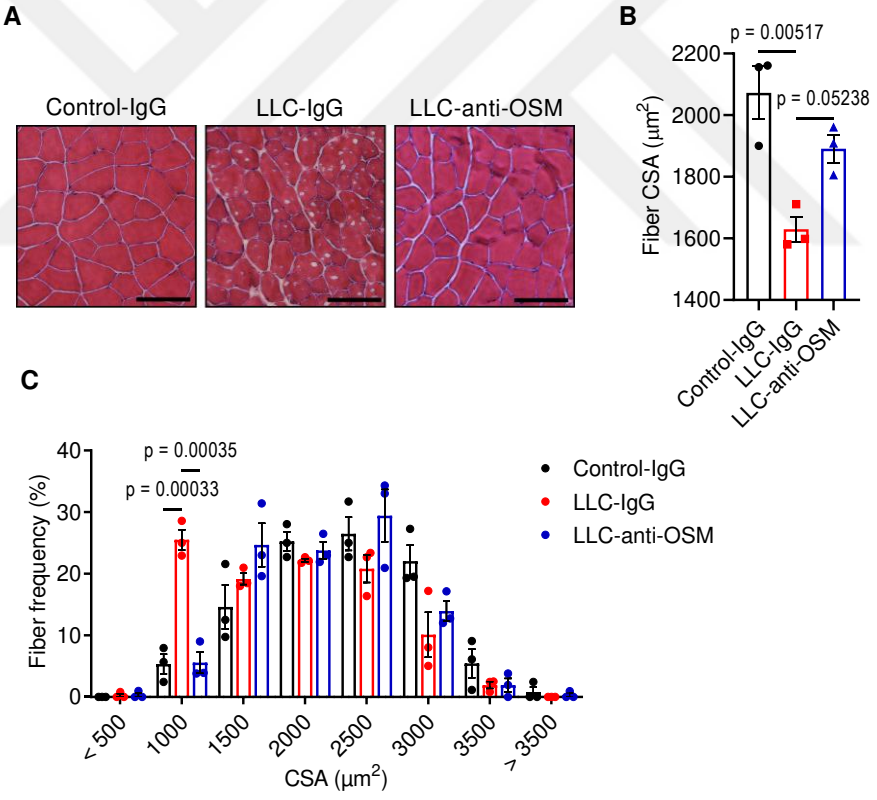

Figure 3-28: Fiber area and frequency of muscles are rescued upon OSM neutralization in cachectic mice. **(A)** LLC tumor cells were injected to mice, IgG and anti-OSM antibodies (1mg/kg) were administered. Mice were sacrificed and muscle tissues were collected, sectioned and H&E stained. **(B)** Fiber cross-sectional area and **(C)** frequency were calculated. Data are presented as individual measurements (points) and

mean ± SEM. Statistical analysis was conducted using 1-way ANOVA with Tukey's post hoc test. Fiber frequency measurements were performed by Samet Ağca.

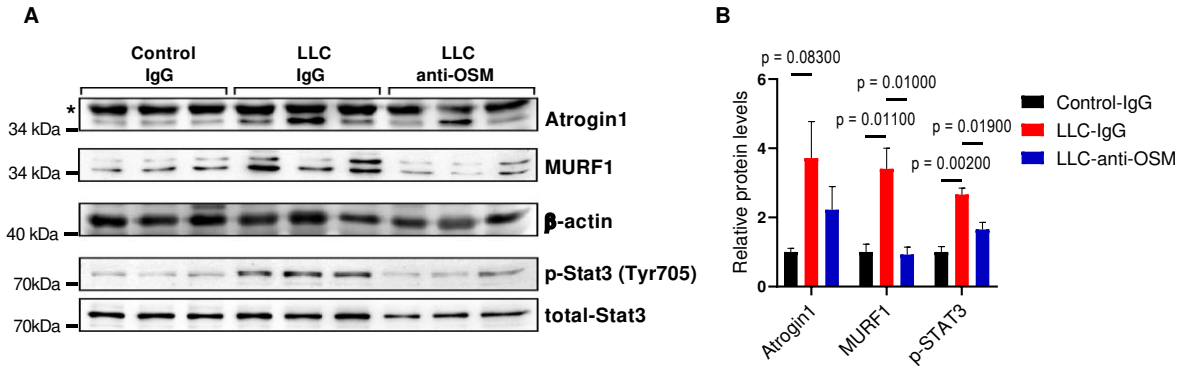

Figure 3-29: High protein levels of atrophy markers are reduced upon OSM neutralization in cachectic mice (A) LLC tumor cells were injected to mice, IgG and anti-OSM antibodies (1mg/kg) were administered. Protein levels were determined via western blotting. Asterisks (*) determines the nonspecific band. **(B)** The band intensities were quantified. Statistical analysis was conducted using 1-way ANOVA with Tukey's post hoc test.

3.9 The Immune System is the Probable Source of Tumor-Induced OSM

High OSM levels are present in tumor-bearing cachectic mice (Bilgic et al., 2023). Similarly, a previous study (Bonetto et al., 2011) detected serum OSM in C26 tumor-bearing mice with moderate (121 pg/ml) and severe cachexia (220 pg/ml). The involvement of OSM in numerous inflammatory disorders indicates that the persistent activation of the immune system may be the source of systemic OSM (Wolf et al., 2023). To understand the source of tumor-induced OSM leading to cachexia-driven muscle atrophy, we used mice with severe combined immunodeficiency (SCID). We inoculated LLC tumor cells to the SCID mice and sacrificed after 16 days. OSM was not present in the plasma of LLC-injected SCID mice. However, there was still cachectic atrophy present in mice supporting the fact that cachexia is a multifactorial disorder. The SCID mice had significantly reduced muscle weight and strength compared to the control group. Overall, OSM absence in the plasma of these mice supports the fact that the immune system is likely the source of tumor-induced OSM (Figure 3-25).

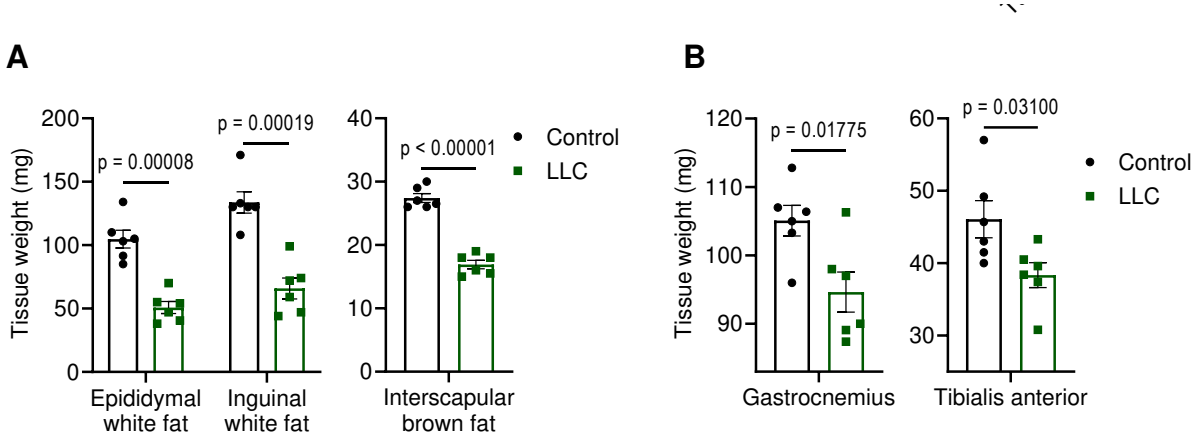

Figure 3-30: Tumors are not the source of atrophy-inducer OSM. (A-B) LLC (5 million cells) were inoculated to severe combined immunodeficiency (SCID) mice, and they were sacrificed 16 days post-tumor injection. Adipose **(A)** and muscle **(B)** tissues were weighed (n = 6). Data are presented as individual measurements (points) and mean ± SEM. Statistical analysis was conducted using a two-tailed t-test.

3.10 OSMR is Upregulated in Cancer Patients and Muscles of Patients with Muscular Dystrophy

At the clinical level, we wanted to examine if OSM/OSMR signaling is related to muscle wasting in humans. To test this, we analyzed GEO Omnibus Databases and checked the expression of the *OSMR* gene as the chief target of OSM/OSMR signaling in muscle biopsies of weight-losing pancreatic ductal adenocarcinoma (PDAC) patients. This database of microarray analysis, compared by Judge et al. (2018), was composed of 17 cachectic PDAC patients, 5 non-cachectic PDAC patients and 16 noncancer controls. Results showed that *OSMR* expression was upregulated in cachectic PDAC patients compared to non-cancer controls and non-cachectic PDAC patients (in Figure 3-31A). Moreover, we also analyzed if the expression of OSM-target genes identified by RNA sequencing are enriched in these samples. We performed gene set enrichment analysis (GSEA) of top 200 genes upregulated by OSM and compared their expression in the muscle biopsies of cachectic PDAC patients (Figure 3-31B). The results show that OSM target genes were significantly expressed in muscle biopsies of cachectic PDAC patients.

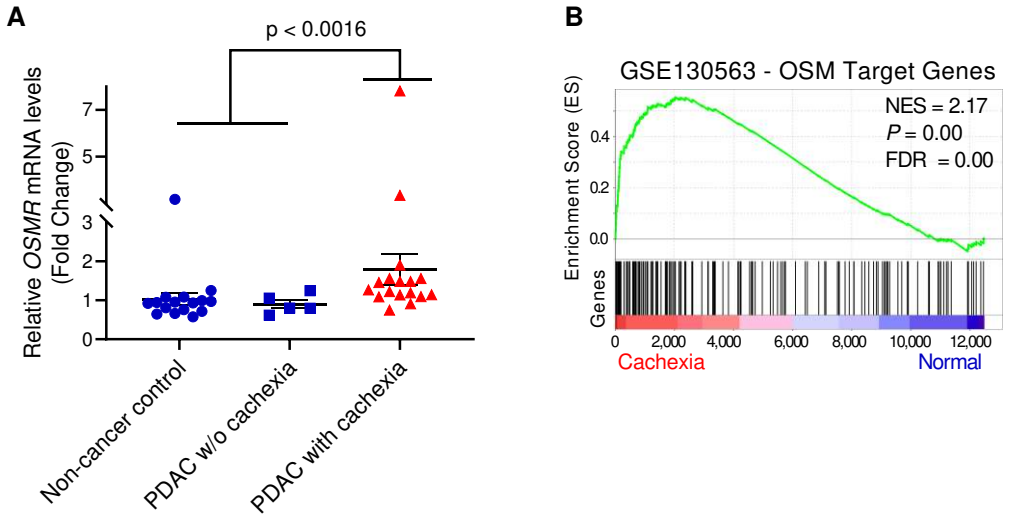

Figure 3-31: OSMR and its target genes are upregulated in PDAC cachectic patients. **(A)** GEO2R analysis of OSMR expression levels between normal subjects and PDAC patients (GSE130563) (n = 16 for non-cancer controls, n = 5 for non-cachectic PDAC patients, and n = 17 for cachectic PDAC patients). **(B)** GSEA of the top 200 OSM target genes between cachectic PDAC patients with non-cancer controls and non-cachectic PDAC patients was performed (GEO: GSE130563). Analysis was performed by Samet Ağca.

In GEO database analysis, we also confirmed an upregulated expression of *OSMR* in patients with muscular dystrophy. *OSMR* is upregulated in patients with Duchenne muscular dystrophy (DMD) and facioscapulohumeral muscular dystrophy (FSHD) (Figure 3-32). The analysis of gene expression profiles of muscle biopsies from 10 DMD patients and 11 unaffected subjects studied by Haslett et al. (2003) (GEO: GSE1007) revealed an increase in *OSMR* levels in DMD patients (Figure 3-32A). *OSMR* transcripts are shown to be upregulated also in patients with FSHD. In a study by Wang et al. (2019) (GSE115650) the muscle biopsies from patients were collected to analyze the expression of target genes of double homeobox 4 (DUX4), which is abnormally expressed in muscle and associated with this disease. The patients were separated into 4 groups according to the expression of these markers (From the lowest to the highest expression levels). Compared to 9 control subjects, *OSMR* transcript levels were elevated in 34 FSHD patients of all groups (Figure 3-32B). Moreover, the follow-up studies were published for the same patients (GEO: GSE140261) in which *OSMR* transcript levels remained elevated (n = 27) (Figure 3-32C). We also tested OSM top 200 target gene expression levels in these databases using GSEA analysis (Figure 3-32D, E and F). *OSMR* and OSM top target

genes were significantly enriched in the muscular dystrophies pointing out the fact that OSM/OSMR signaling is not limited only to cachexia-driven muscle wasting.

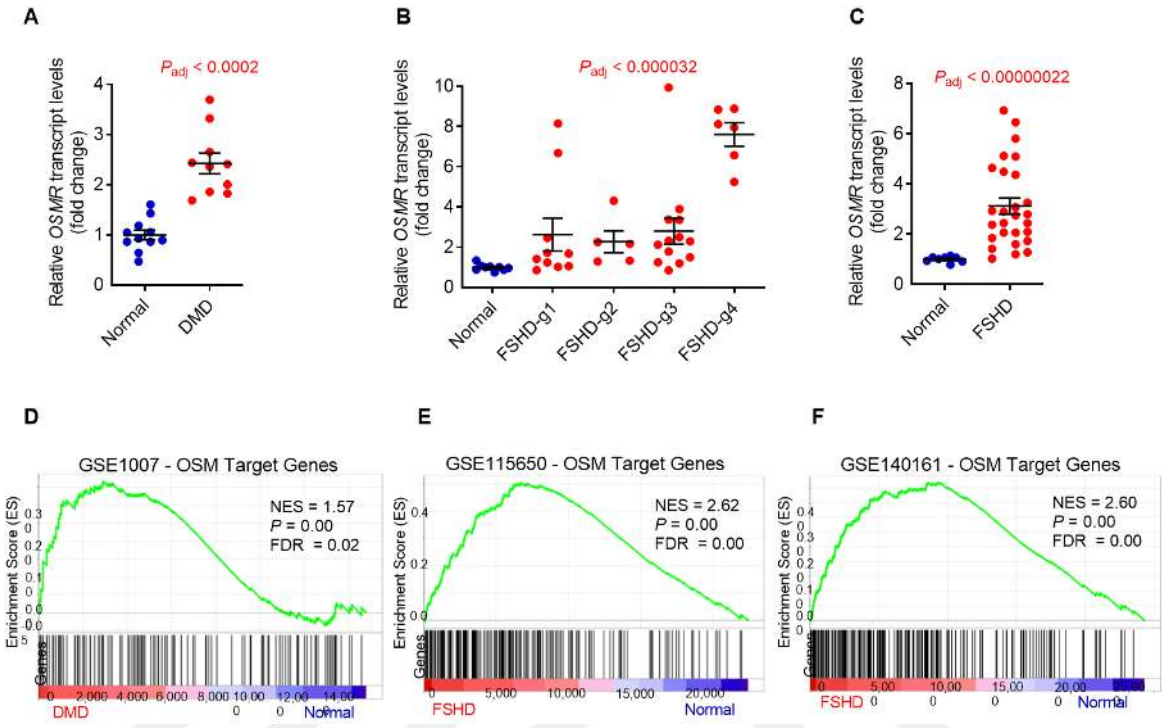

Figure 3-32: OSMR transcript levels are upregulated in DMD and FSHD patients. **(A)** OSMR expression values of normal subjects and DMD patients were analyzed by GEO2R (GSE1007) (n = 11 for normal subjects, n = 10 for DMD subjects) **(B-C)** OSMR expression values of normal subjects and FSHD patients were analyzed by DESeq2 **(B)** (GSE115650) (n = 9 for normal subjects, n = 34 for FSHD subjects). **(C)** (GSE140261) (n = 8 for normal subjects, n = 27 for FSHD subjects). (D-F) GSEA analysis was performed for each database.

Apart from DMD and FSHD, *OSMR* expression is also upregulated in other muscular disorders (Figure 3-33). 49 muscle biopsies from patients with DMD, Becker muscular dystrophy (BMD) and limb-girdle muscular dystrophy (LGMD) were investigated from a GEO database (Dadgar et al., 2014). Analysis of this dataset (GEO: GSE109178) showed that *OSMR* transcript is elevated in patients with DMD (n = 17), BMD (n = 11), and dysferlin-deficient LGMD2B (n = 8) compared to normal subjects (n = 6) (Figure 3-33A). Moreover, Analysis of the dataset (GEO: GSE3307) showed OSMR upregulation in patients with DMD (n = 10), BMD (n = 5), acute quadriplegic myopathy (n = 5), FSHD (n = 14), juvenile dermatomyositis (JDM) (n = 21), calpain3-deficient LGMD2A (n = 10), dysferlin-deficient LGMD2B (n = 11), and fukutin-related protein-

deficient LGMD2I (n = 7) compared to normal subjects (n = 18) (Figure 3-33B). Overall, the results show that OSM/OSMR signaling is activated in various muscular disorders. Targeting OSM/OSMR signaling can benefit many muscular disorders.

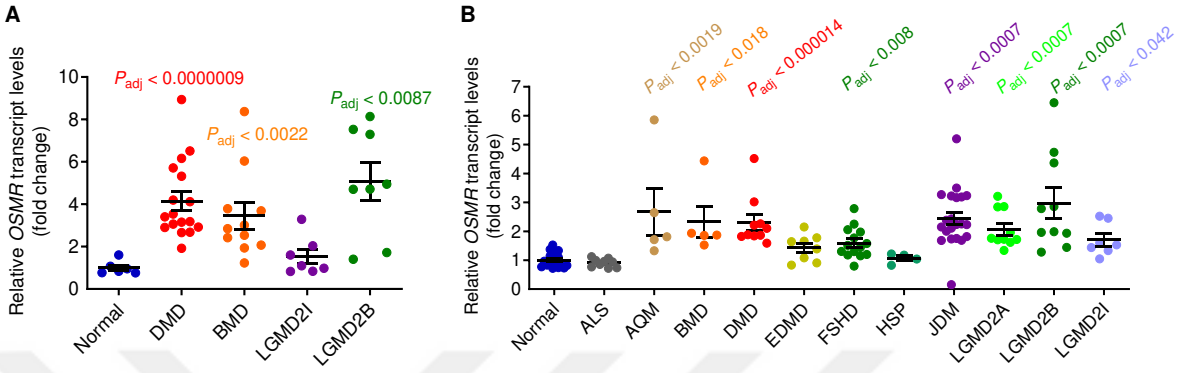

Figure 3-33: OSMR transcript levels are upregulated in patients with muscular dystrophy. (A) The OSMR expression values of control group and DMD patients were analyzed by GEO2R (GSE109178) (n = 6 for normal subjects, n = 17 for DMD subjects, n = 11 for Becker muscular dystrophy (BMD) subjects, n = 7 for fukutin-related protein (FKRP)-deficient limb girdle muscular dystrophy type 2I (LGMD2I) subjects and n = 8 for dysferlin-deficient limbgirdle muscular dystrophy type 2B (LGMD2B) subjects). **(B)** GEO2R analysis (GSE3307) of OSMR transcript levels of normal subjects and muscular dystrophy patients (n = 18 for normal subjects, n = 9 for amyotrophic lateral sclerosis (ALS) patients, n = 5 for acute quadriplegic myopathy (AQM), n = 5 for Becker muscular dystrophy (BMD) patients, n = 10 for DMD patients, n = 8 for Emery Dreifuss muscular dystrophy (EDMD) patients, n = 14 for FSHD patients, n = 4 for hereditary spastic paraplegia (HSP) patients, n = 21 for juvenile dermatomyositis (JDM) patients, n = 10 for calpain3-deficient limb-girdle muscular dystrophy type 2A (LGMD2A) patients, n = 10 for dysferlin-deficient limb-girdle muscular dystrophy type 2B (LGMD2B) patients, and n = 7 for fukutin-related protein (FKRP)-deficient limb girdle muscular dystrophy type 2I (LGMD2I) patients).

Chapter 4: DISCUSSION

Cachexia is a debilitating syndrome associated with excessive muscle and fat loss. Skeletal muscle atrophy, as a hallmark of cachexia, accompanies many disorders, primarily cancer. More than half of cancer patients suffer from cachexia and 20% of deaths occur in cachectic cancer patients. The exact mechanism behind cachexia-driven muscle loss is elusive. Multiple cytokine-signaling pathways are activated upon muscle wasting. Several proteins are identified as mediators of cachexia. However, pre-clinical stages have mostly failed to prevent cachectic weight and muscle loss. Therefore, successful therapies against cachexia-leading muscle loss have become an unmet medical need (Dolly et al., 2020).

Certain studies have focused on mitigating the effects of cachexia by blocking inflammatory cytokines, such as TNFα. However, potential therapies with TNFα inhibitors (e.g., infliximab or etanercept) failed to prevent muscle loss (Domaniku et al., 2023). Infliximab, the monoclonal antibody against TNFα, was reported to have adverse effects with a significant increase in body weight and body mass index (BMI) (Patsalos et al., 2020).

Beyond TNFα, other cytokines like IL-1, IL-6 and LIF proteins have been identified as drivers of muscle loss. Recent studies focused on certain therapeutic targets against IL-1 and IL-6 but failed to prevent cachexia-driven body loss. IL-1 specific monoclonal antibody xilonix (MABp1) improved the body mass of only responding cachectic patients. The anti-IL-6 antibody approach reversed muscle loss in cachectic mice, however, the trial of ALD518 (a humanized IL-6 monoclonal antibody) failed to improve the lean body mass of nonsmall-cell lung cancer (NSCLC) patients (Domaniku et al., 2023).

Pre-clinical studies using activin A decoy receptor or human monoclonal anti-ActR2 antibody showed positive results in maintaining lean body mass. Moreover, the combination therapy with activin A decoy receptor and ghrelin receptor agonist Anarelin, known to improve appetite and body weight, reversed muscle loss in cachectic mice. Blocking Activin A rescued muscle loss in a sex-dependent manner (Queiroz et al., 2022). However, clinical trials with anti-myostatin antibodies on pancreatic cancer patients have been discontinued due to deleterious effects on patients' survival (Golan et al., 2018).

GDF15, a stress hormone, is another recently identified cachexia-causing agent. Anti-GDF15 antibodies successfully reversed the cachectic condition in mice (Kim-Muller et al., 2023; Suriben et al., 2020) giving hopeful insights for future clinical trials in humans. However, GDF15 also shows a protective role against inflammation by maintaining tissue tolerance through the regulation of triglyceride metabolism (Luan et al., 2019). This requires careful examination of cachectic patients getting GDF15-GFRAL antagonists since they are more susceptible to any kind of infection (Lockhart et al., 2020).

While previous efforts to combat cachexia have not been fully successful, emerging research on Oncostatin M offers a promising new approach for addressing muscle wasting in cachectic conditions. OSM is shown to induce cellular atrophy in C2C12 myotubes (Miki et al., 2019). Our study shows that via JAK2/STAT3 pathway activation, OSM induces shrinkage of primary myotubes in vitro. OSM upregulates its top-list genes, which are associated with muscle atrophy. *Serpina3n*, as the top target of OSM, is a serine protease upregulated in damaged muscle tissues, C26 (colon carcinoma) cachectic murine models, but also during glucocorticoid-related muscle atrophy (Gueugneau et al., 2018; Shum et al., 2015; Tjondrokoesoemo et al., 2016). Moreover, *Ampd3, Sln, Mt1, Mt2, Cebpd*, and *Igfbp3* were also identified as potential atrophy markers. *Ampd3* regulates the ratio between adenine nucleotide content and ATP, contributing significantly to the balance of muscle metabolism. There was an increase in *Ampd3* levels observed in muscles experiencing atrophy (Brocca et al., 2017; Ibebunjo et al., 2013; Lecker et al., 2004). *Cebpd* (CAAT/enhancer binding protein d) expression levels are elevated in glucocorticoid-induced atrophy conditions (Yang et al., 2005). *Igfbp3* codes for a protein that binds to insulin-like growth factor (IGF), demonstrated to inhibit IGF signaling and stimulate atrophy in C2C12 myotubes. Elevated *Igfbp3* levels were observed in the muscles of mice with tumors (Cole et al., 2021; Huang et al., 2016). *Mt1* and *Mt2* are metallothioneins whose expression is elevated in murine and human muscles undergoing wasting (Lecker et al., 2004; Urso et al., 2007; Urso et al., 2006). *Sln* expression levels are elevated during muscular dystrophy (Voit et al., 2017).

OSM overexpression triggers significant muscle wasting in vivo. Studies have shown that OSM overexpression upon adeno-associated virus transduction had shrunk muscles in mice (Jengelley et al., 2022). In the study by Bilgic et al. (2023) , the atrophy-inducer OSM's mechanism of action was investigated. Primarily, OSM activates the

EDA2R/NIK signaling pathway to induce atrophy. In vitro, OSM overexpression or recombinant OSM treatment induces Eda2r expression in primary myotubes (Bilgic et al., 2023). High ectodysplasin A2 receptor (EDA2R) expression in muscle is associated with cancer cachexia, denervation, aging and muscular dystrophies (Ozen & Kir, 2024). In primary myotubes, OSM, together with EDA-A2, additively promotes cellular atrophy. Bilgic et al. (2023) concluded that tumor-induced OSM elevates EDA2R expression in muscle; when OSMR is deficient in muscle, the wasting gets blunted. Therefore, OSM/OSMR and EDA2R/NIK signaling act in parallel to induce muscle wasting.

To better mark the importance of OSM in tumor-induced muscle loss, the OSMR-muscle-specific deleted mice were inoculated with LLC and B16 cancer cells. Muscle-specific depleted OSMR tumor-bearing mice rescued atrophy and showed improved muscle function. Mice improved their whole limb hanging and forelimb muscle strength. Moreover, OSM blockade by anti-OSM antibodies also protected tumor-bearing mice from cachexia-driven muscle loss. The OSM neutralization experiments phenocopied the muscle-OSMR depletion results. However, the muscle strength upon antibody administration did not fully rescue the effect in tumor-bearing mice. This shows that further nutritional changes and further exercise plans may help in restoring muscle strength.

The source of OSM in inducing muscle wasting is not clear. Literature shows that the C2C12 myotubes do not express OSM (Xiao et al., 2011). Our data has indicated that cachexia-inducing tumor inoculation increases OSM levels in plasma of mice. However, our results demonstrated that OSM is not expressed by tumor cells or muscle tissue. Therefore, we argue that OSM secretion is likely carried out by other cell types located either inside or outside the tumor microenvironment, such as immune cells, cancer-associated fibroblasts or endothelial cells. In fact, tumors might affect OSM secretion indirectly through triggering inflammation, as a general feature of cancer cachexia. Our data shows that OSM is undetectable in the plasma of immunodeficient tumor-bearing SCID mice. So, we speculate that the immune system is the possible source of OSM secretion. In a recent study by Dollet et al., authors suggested inflammation to be the source of OSM in triggering exercise-induced lipolysis. Acute exercise promoted the secretion of factors from muscle tissue, which activated inflammatory cells (monocyte/macrophages and T cells). These inflammatory cells were indicated to release OSM in adipose tissue triggering lipolysis (Dollet et al., 2024). Similarly, during cancer

cachexia, tumor-derived factors may persistently activate immune cells, driving their infiltration into host tissues and leading to the secretion of atrophy-inducer OSM, which upregulates expression of OSMR and other atrophy-related genes in muscle. While OSM expression is not detectable in muscle tissue, further studies should test OSM levels in immune cell fractions of the tumor-bearing mice. For this purpose, flow cytometry can be used to identify the specific cell types secreting OSM. OSM/OSMR signaling activation seems to contribute to many muscle disorders; therefore, understanding the source of OSM during cancer cachexia can reveal the source of OSM in promoting high OSMR expression and also in other muscular dystrophies.

The Oncostatin M / Oncostatin M receptor (OSM/OSMR) angle provides a new target for mitigating cachexia-driven muscle loss (Figure 4-1). Therapeutic approaches to block OSM signaling have been demonstrated with anti-OSM antibodies. A monoclonal OSM antibody (GSK315234) is used in Phase II clinical trials for patients with Rheumatoid Arthritis (Choy et al, 2013). GSK-OSM has a dose-dependent neutralizing effect on OSM; high-dose antibody-OSM binding increases the half-life of OSM, however, it has lower binding affinity than OSM and its receptor, OSMR. Further experiments on the dissociation rate of antibody-OSM should be examined. A recent humanized monoclonal anti-OSM antibody (GSK2330811) is tested for the treatment of inflammatory and fibrotic diseases, such as systemic sclerosis (Richards & Botelho, 2019). However, the Phase II studies with this antibody showed no significant change compared to the placebo (Denton et al., 2022). Another study used Vixarelimab, an antibody against the beta subunit of the Oncostatin M receptor (OSMR), for treatment of Prurigo nodularis (a chronic skin disease). In Phase IIa studies, this antibody resulted in almost-clear skin and reduced itches in patients giving promising results for further clinical examinations (Sofen et al., 2023). Such therapeutic tools can be used to ameliorate the effect of OSM/OSMR signaling in various diseases.

In general, the IL-6 family members IL-6, LIF and OSM have an overlapping role in contributing to the development of cancer cachexia and other disease pathogenesis. If therapeutic agents target all three cytokines simultaneously, more favorable outcomes may be obtained. For example, JAK2 kinase inhibitors Ruxolitinib and Tofacitinib have shown promising results on rescuing cachexia in mice (Arora et al, 2020). Currently, Ruxolitinib is tested in Phase II clinical trials to evaluate its effect on preventing cytokine-triggered muscle wasting in NSCLC patients (NCT04906746). Since not only these

cytokines use the JAK/STAT signaling, the possible adverse effect on blocking the whole pathway should be considered. Moreover, another targeting strategy would be considering gp130 blockage. Similarly, since gp130 is also the hub of many signaling networks and its complete blockage can result in many side effects, therapies should aim to reduce activation of gp130 downstream signaling to normal levels. Certain studies are being performed with orally active small molecule SC144 as the first-in-class potent gp130 inhibitor which will serve information for further clinical examinations (Xu & Neamati, 2013). Studies have shown that anti-IL-6 antibodies are not sufficient to inhibit myeloma growth and this can be overcome using antibodies against gp130 (Burger et al., 2017).

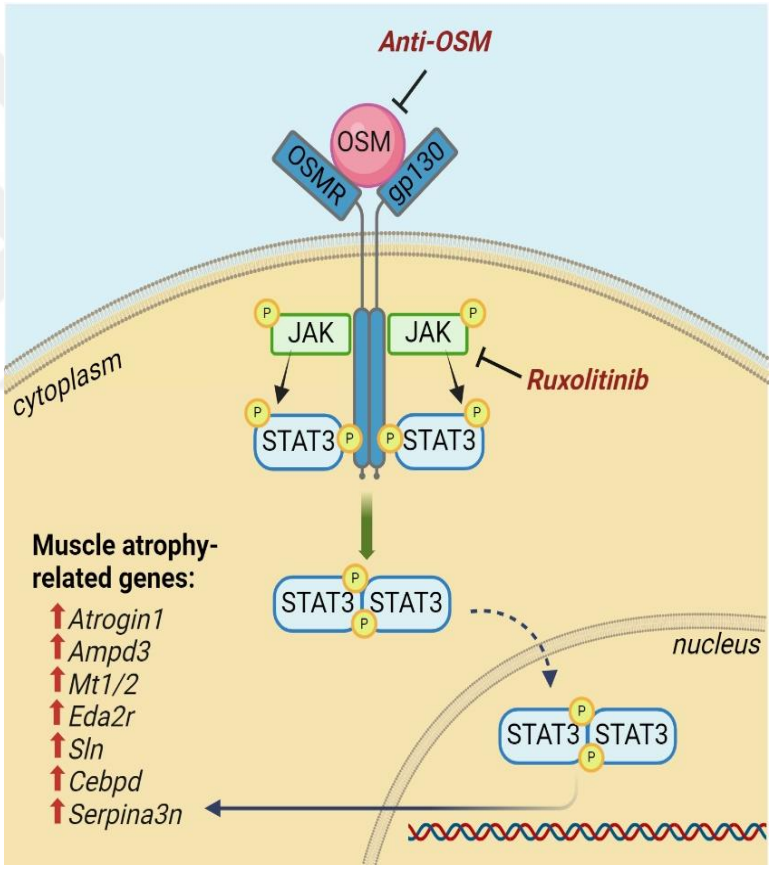

Figure 4-1: The OSM/OSMR signaling cascade in cachexia. OSM binds to its OSMR/gp130 receptor and activates the JAK/STAT3 pathway. JAK kinases bind to the receptors and auto-phosphorylate to recruit STAT molecules. The activated STAT3 molecules homodimerize and move into the nucleus to induce the expression of muscle atrophy. Anti-OSM antibody or Ruxolitinib, a JAK1/2 inhibitor, can be used to block the cascade (Adapted from Domaniku et al. (2023)).

Chapter 5: SUMMARY

Our study has revealed the effect of OSM/OSMR signaling in inducing muscle loss. OSM activates JAK/STAT3 pathway to induce muscle wasting both in vitro and in vivo. OSM elevates the expression of atrophy markers and the related genes, and its overexpression induces muscle atrophy via the JAK/STAT3 pathway. High OSMR transcript levels are found in many muscular disorders.

Overall, our findings emphasize the promising potential of targeting the OSM/OSMR pathway as an effective therapeutic strategy for alleviating muscle atrophy. By strategically intervening in this signaling pathway either by chemical inhibition, receptor deletion or antibody administration, it might be feasible to effectively halt the progression of muscle loss, thereby creating new opportunities for addressing this devastating condition.

BIBLIOGRAPHY

Argiles, J. M., Betancourt, A., Guardia-Olmos, J., Pero-Cebollero, M., Lopez-Soriano, F. J., Madeddu, C., Serpe, R., & Busquets, S. (2017). Validation of the CAchexia SCOre (CASCO). Staging Cancer Patients: The Use of miniCASCO as a Simplified Tool. *Front Physiol*, *8*, 92. https://doi.org/10.3389/fphys.2017.00092

Argiles, J. M., Busquets, S., Stemmler, B., & Lopez-Soriano, F. J. (2014). Cancer cachexia: understanding the molecular basis. *Nat Rev Cancer*, *14*(11), 754-762. https://doi.org/10.1038/nrc3829

Argiles, J. M., Lopez-Soriano, F. J., Stemmler, B., & Busquets, S. (2023). Cancer-associated cachexia - understanding the tumour macroenvironment and microenvironment to improve management. *Nat Rev Clin Oncol*, *20*(4), 250-264. https://doi.org/10.1038/s41571-023-00734-5

Aversa, Z., Pin, F., Lucia, S., Penna, F., Verzaro, R., Fazi, M., Colasante, G., Tirone, A., Rossi Fanelli, F., Ramaccini, C., Costelli, P., & Muscaritoli, M. (2016). Autophagy is induced in the skeletal muscle of cachectic cancer patients. *Sci Rep*, *6*, 30340. https://doi.org/10.1038/srep30340

Babon, J. J., Varghese, L. N., & Nicola, N. A. (2014). Inhibition of IL-6 family cytokines by SOCS3. *Semin Immunol*, *26*(1), 13-19. https://doi.org/10.1016/j.smim.2013.12.004

Bachmann J., H. M., Krakowski-Roosen H., Büchler M.W., Friess H., Martignoni M.E. (2008).

Baracos, V. E., Martin, L., Korc, M., Guttridge, D. C., & Fearon, K. C. H. (2018). Cancer-associated cachexia. *Nat Rev Dis Primers*, *4*, 17105. https://doi.org/10.1038/nrdp.2017.105

Bayliss, T., Smith, J., Schuster, M.,, & Dragnev, K., Rigas, J. (2011). A humanized anti-IL-6 antibody (ALD518) in non-small cell lung cancer. *Drug Evaluation*.

Bilgic, S. N., Domaniku, A., Toledo, B., Agca, S., Weber, B. Z. C., Arabaci, D. H., Ozornek, Z., Lause, P., Thissen, J. P., Loumaye, A., & Kir, S. (2023). EDA2R-NIK signalling promotes muscle atrophy linked to cancer cachexia. *Nature*, *617*(7962), 827-834. https://doi.org/10.1038/s41586-023-06047-y

Bindels, A. M. N., Audrey Loumaye2, Emilie Catry1, Hannah, Walgrave1, C. C., Sophie Leclercq1,4, Matthias Van Hul1,5, Hubert, Plovier1, Barbara Pachikian1, Luis G. Bermúdez-Humarán3, Philippe Langella3,, & Patrice D. Cani1, Jean-Paul Thissen2 and Nathalie M. Delzenne1. (2018). Increased gut permeability in cancer cachexia: mechanisms and

clinical relevance.

Bonaldo, P., & Sandri, M. (2013). Cellular and molecular mechanisms of muscle atrophy. *Dis Model Mech*, *6*(1), 25-39. https://doi.org/10.1242/dmm.010389

Bonetto, A., Aydogdu, T., Jin, X., Zhang, Z., Zhan, R., Puzis, L., Koniaris, L. G., & Zimmers, T. A. (2012). JAK/STAT3 pathway inhibition blocks skeletal muscle wasting downstream of IL-6 and in experimental cancer cachexia. *Am J Physiol Endocrinol Metab*, *303*(3), E410-421. https://doi.org/10.1152/ajpendo.00039.2012

Bonetto, A., Aydogdu, T., Kunzevitzky, N., Guttridge, D. C., Khuri, S., Koniaris, L. G., & Zimmers, T. A. (2011). STAT3 activation in skeletal muscle links muscle wasting and the acute phase response in cancer cachexia. *PLoS One*, *6*(7), e22538. https://doi.org/10.1371/journal.pone.0022538

Brocca, L., Toniolo, L., Reggiani, C., Bottinelli, R., Sandri, M., & Pellegrino, M. A. (2017). FoxO-dependent atrogenes vary among catabolic conditions and play a key role in muscle atrophy induced by hindlimb suspension. *J Physiol*, *595*(4), 1143-1158. https://doi.org/10.1113/JP273097

Burger, R., Gunther, A., Klausz, K., Staudinger, M., Peipp, M., Penas, E. M., Rose-John, S., Wijdenes, J., & Gramatzki, M. (2017). Due to interleukin-6 type cytokine redundancy only glycoprotein 130 receptor blockade efficiently inhibits myeloma growth. *Haematologica*, *102*(2), 381-390. https://doi.org/10.3324/haematol.2016.145060

Chollangi, S., Mather, T., Rodgers, K. K., & Ash, J. D. (2012). A unique loop structure in oncostatin M determines binding affinity toward oncostatin M receptor and leukemia inhibitory factor receptor. *J Biol Chem*, *287*(39), 32848-32859. https://doi.org/10.1074/jbc.M112.387324

Cohen, S., Nathan, J. A., & Goldberg, A. L. (2015). Muscle wasting in disease: molecular mechanisms and promising therapies. *Nat Rev Drug Discov*, *14*(1), 58-74. https://doi.org/10.1038/nrd4467

Cole, C. L., Bachman, J. F., Ye, J., Murphy, J., Gerber, S. A., Beck, C. A., Boyce, B. F., Muthukrishnan, G., Chakkalakal, J. V., Schwarz, E. M., & Linehan, D. (2021). Increased myocellular lipid and IGFBP-3 expression in a pre-clinical model of pancreatic cancer-related skeletal muscle wasting. *J Cachexia Sarcopenia Muscle*, *12*(3), 731-745. https://doi.org/10.1002/jcsm.12699

Dadgar, S., Wang, Z., Johnston, H., Kesari, A., Nagaraju, K., Chen, Y. W., Hill, D. A., Partridge, T. A., Giri, M., Freishtat, R. J., Nazarian, J., Xuan, J., Wang, Y., & Hoffman, E. P. (2014). Asynchronous remodeling is a driver of failed regeneration in Duchenne muscular dystrophy. *J Cell Biol*, *207*(1), 139-158. https://doi.org/10.1083/jcb.201402079

Das, S. K., Eder, S., Schauer, S., Diwoky, C., Temmel, H., Guertl, B., Gorkiewicz, G., Tamilarasan, K. P., Kumari, P., Trauner, M., Zimmermann, R., Vesely, P., Haemmerle, G., Zechner, R., & Hoefler, G. (2011). Adipose Triglyceride Lipase Contributes to Cancer-Associated Cachexia. *Science*, *333*(6039), 233-238. https://doi.org/doi:10.1126/science.1198973

De Paepe, B. (2020). Progressive Skeletal Muscle Atrophy in Muscular Dystrophies: A Role for Toll-like Receptor-Signaling in Disease Pathogenesis. *Int J Mol Sci*, *21*(12). https://doi.org/10.3390/ijms21124440

Denton, C. P., Del Galdo, F., Khanna, D., Vonk, M. C., Chung, L., Johnson, S. R., Varga, J., Furst, D. E., Temple, J., Zecchin, C., Csomor, E., Lee, A., Wisniacki, N., Flint, S. M., & Reid, J. (2022). Biological and clinical insights from a randomized phase 2 study of an anti-oncostatin M monoclonal antibody in systemic sclerosis. *Rheumatology (Oxford)*, *62*(1), 234-242. https://doi.org/10.1093/rheumatology/keac300

Dodington, D. W., Desai, H. R., & Woo, M. (2018). JAK/STAT - Emerging Players in Metabolism. *Trends Endocrinol Metab*, *29*(1), 55-65. https://doi.org/10.1016/j.tem.2017.11.001

Dollet, L., Lundell, L. S., Chibalin, A. V., Pendergrast, L. A., Pillon, N. J., Lansbury, E. L., Elmastas, M., Frendo-Cumbo, S., Jalkanen, J., de Castro Barbosa, T., Cervone, D. T., Caidahl, K., Dmytriyeva, O., Deshmukh, A. S., Barres, R., Ryden, M., Wallberg-Henriksson, H., Zierath, J. R., & Krook, A. (2024). Exercise-induced crosstalk between immune cells and adipocytes in humans: Role of oncostatin-M. *Cell Rep Med*, *5*(1), 101348. https://doi.org/10.1016/j.xcrm.2023.101348

Dolly, A., Dumas, J. F., & Servais, S. (2020). Cancer cachexia and skeletal muscle atrophy in clinical studies: what do we really know? *J Cachexia Sarcopenia Muscle*, *11*(6), 1413-1428. https://doi.org/10.1002/jcsm.12633

Domaniku, A., Bilgic, S. N., & Kir, S. (2023). Muscle wasting: emerging pathways and potential drug targets. *Trends Pharmacol Sci*, *44*(10), 705-718. https://doi.org/10.1016/j.tips.2023.07.006

Eskiler, G. G., Bezdegumeli, E., Ozman, Z., Ozkan, A. D., Bilir, C., Kucukakca, B. N., Ince, M. N., Men, A. Y., Aktas, O., Horoz, Y. E., Akpinar, D., Genc, I., & Kaleli, S. (2019). IL-6 mediated JAK/STAT3 signaling pathway in cancer patients with cachexia. *Bratisl Lek Listy*, *66*(11), 819-826. https://doi.org/10.4149/BLL_2019_136

Evans, W. J., Morley, J. E., Argiles, J., Bales, C., Baracos, V., Guttridge, D., Jatoi, A., Kalantar-Zadeh, K., Lochs, H., Mantovani, G., Marks, D., Mitch, W. E., Muscaritoli, M., Najand, A., Ponikowski, P., Rossi Fanelli, F., Schambelan, M., Schols, A., Schuster, M., . . . Anker, S. D. (2008). Cachexia: a new definition. *Clin Nutr*, *27*(6), 793-799. https://doi.org/10.1016/j.clnu.2008.06.013

Fearon, K. C., Glass, D. J., & Guttridge, D. C. (2012). Cancer cachexia: mediators, signaling, and metabolic pathways. *Cell Metab*, *16*(2), 153-166. https://doi.org/10.1016/j.cmet.2012.06.011

Febbraio, M. A. (2007). gp130 receptor ligands as potential therapeutic targets for obesity. *J Clin Invest*, *117*(4), 841-849. https://doi.org/10.1172/JCI30453

Ferrara, M., Samaden, M., Ruggieri, E., & Venereau, E. (2022). Cancer cachexia as a multiorgan failure: Reconstruction of the crime scene. *Front Cell Dev Biol*, *10*, 960341. https://doi.org/10.3389/fcell.2022.960341

Ferrer, M., Anthony, T. G., Ayres, J. S., Biffi, G., Brown, J. C., Caan, B. J., Cespedes Feliciano, E. M., Coll, A. P., Dunne, R. F., Goncalves, M. D., Grethlein, J., Heymsfield, S. B., Hui, S., Jamal-Hanjani, M., Lam, J. M., Lewis, D. Y., McCandlish, D., Mustian, K. M., O'Rahilly, S., . . . Janowitz, T. (2023). Cachexia: A systemic consequence of progressive, unresolved disease. *Cell*, *186*(9), 1824-1845. https://doi.org/10.1016/j.cell.2023.03.028

Furrer, R., & Handschin, C. (2019). Muscle Wasting Diseases: Novel Targets and Treatments. *Annu Rev Pharmacol Toxicol*, *59*, 315-339. https://doi.org/10.1146/annurev-pharmtox-010818-021041

Golan, T., Geva, R., Richards, D., Madhusudan, S., Lin, B. K., Wang, H. T., Walgren, R. A., & Stemmer, S. M. (2018). LY2495655, an antimyostatin antibody, in pancreatic cancer: a randomized, phase 2 trial. *J Cachexia Sarcopenia Muscle*, *9*(5), 871-879. https://doi.org/10.1002/jcsm.12331

Gueugneau, M., d'Hose, D., Barbe, C., de Barsy, M., Lause, P., Maiter, D., Bindels, L. B., Delzenne, N. M., Schaeffer, L., Gangloff, Y. G., Chambon, C., Coudy-Gandilhon, C., Bechet, D., & Thissen, J. P. (2018). Increased Serpina3n release into circulation during glucocorticoid-mediated muscle atrophy. *J Cachexia Sarcopenia Muscle*, *9*(5), 929-946. https://doi.org/10.1002/jcsm.12315

Haslett, J. N., Sanoudou, D., Kho, A. T., Han, M., Bennett, R. R., Kohane, I. S., Beggs, A. H., & Kunkel, L. M. (2003). Gene expression profiling of Duchenne muscular dystrophy skeletal muscle. *Neurogenetics*, *4*(4), 163-171. https://doi.org/10.1007/s10048-003-0148-x

Hermanns, H. M. (2015). Oncostatin M and interleukin-31: Cytokines, receptors, signal transduction and physiology. *Cytokine Growth Factor Rev*, *26*(5), 545-558. https://doi.org/10.1016/j.cytogfr.2015.07.006

Hu, X., Li, J., Fu, M., Zhao, X., & Wang, W. (2021). The JAK/STAT signaling pathway: from bench to clinic. *Signal Transduct Target Ther*, *6*(1), 402. https://doi.org/10.1038/s41392-021-00791-1

Huang, X. Y., Huang, Z. L., Yang, J. H., Xu, Y. H., Sun, J. S., Zheng, Q., Wei, C., Song, W., & Yuan, Z. (2016). Pancreatic cancer cell-derived IGFBP-3 contributes to muscle wasting. *J Exp Clin Cancer Res*, *35*, 46. https://doi.org/10.1186/s13046-016-0317-z

Ibebunjo, C., Chick, J. M., Kendall, T., Eash, J. K., Li, C., Zhang, Y., Vickers, C., Wu, Z., Clarke, B. A., Shi, J., Cruz, J., Fournier, B., Brachat, S., Gutzwiller, S., Ma, Q., Markovits, J., Broome, M., Steinkrauss, M., Skuba, E., . . . Glass, D. J. (2013). Genomic and proteomic profiling reveals reduced mitochondrial function and disruption of the neuromuscular junction driving rat sarcopenia. *Mol Cell Biol*, *33*(2), 194-212. https://doi.org/10.1128/MCB.01036-12

Jaskiewicz, A., Domoradzki, T., & Pajak, B. (2020). Targeting the JAK2/STAT3 Pathway-Can We Compare It to the Two Faces of the God Janus? *Int J Mol Sci*, *21*(21). https://doi.org/10.3390/ijms21218261

Jatoi, A., Dakhil, S. R., Nguyen, P. L., Sloan, J. A., Kugler, J. W., Rowland, K. M., Jr., Soori, G. S., Wender, D. B., Fitch, T. R., Novotny, P. J., & Loprinzi, C. L. (2007). A placebo-controlled double blind trial of etanercept for the cancer anorexia/weight loss syndrome: results from N00C1 from the North Central Cancer Treatment Group. *Cancer*, *110*(6), 1396-1403. https://doi.org/10.1002/cncr.22944

Jatoi, A., Ritter, H. L., Dueck, A., Nguyen, P. L., Nikcevich, D. A., Luyun, R. F., Mattar, B. I., & Loprinzi, C. L. (2010). A placebo-controlled, double-blind trial of infliximab for cancer-associated weight loss in elderly and/or poor performance non-small cell lung cancer patients (N01C9). *Lung Cancer*, *68*(2), 234-239. https://doi.org/10.1016/j.lungcan.2009.06.020

Jengelley, D. H. A., Wang, M., Narasimhan, A., Rupert, J. E., Young, A. R., Zhong, X., Horan, D. J., Robling, A. G., Koniaris, L. G., & Zimmers, T. A. (2022). Exogenous Oncostatin M induces Cardiac Dysfunction, Musculoskeletal Atrophy, and Fibrosis. *Cytokine*, *159*, 155972. https://doi.org/10.1016/j.cyto.2022.155972

Jones, S. A., & Jenkins, B. J. (2018). Recent insights into targeting the IL-6 cytokine family in inflammatory diseases and cancer. *Nat Rev Immunol*, *18*(12), 773-789. https://doi.org/10.1038/s41577-018-0066-7

Judge, S. M., Nosacka, R. L., Delitto, D., Gerber, M. H., Cameron, M. E., Trevino, J. G., & Judge, A. R. (2018). Skeletal Muscle Fibrosis in Pancreatic Cancer Patients with Respect to Survival. *JNCI Cancer Spectr*, *2*(3), pky043. https://doi.org/10.1093/jncics/pky043

Kim-Muller, J. Y., Song, L., LaCarubba Paulhus, B., Pashos, E., Li, X., Rinaldi, A., Joaquim, S., Stansfield, J. C., Zhang, J., Robertson, A., Pang, J., Opsahl, A., Boucher, M., Breen, D., Hales, K., Sheikh, A., Wu, Z., & Zhang, B. B. (2023). GDF15 neutralization restores muscle function and physical performance in a mouse model of cancer cachexia. *Cell Rep*, *42*(1), 111947. https://doi.org/10.1016/j.celrep.2022.111947

Kir, S., White, J. P., Kleiner, S., Kazak, L., Cohen, P., Baracos, V. E., & Spiegelman, B. M. (2014). Tumour-derived PTH-related protein triggers adipose tissue browning and cancer cachexia. *Nature*, *513*(7516), 100-104. https://doi.org/10.1038/nature13528

Komori, T., & Morikawa, Y. (2022). Essential roles of the cytokine oncostatin M in crosstalk between muscle fibers and immune cells in skeletal muscle after aerobic

exercise. *J Biol Chem*, *298*(12), 102686. https://doi.org/10.1016/j.jbc.2022.102686

Komori, T., Tanaka, M., Furuta, H., Akamizu, T., Miyajima, A., & Morikawa, Y. (2015). Oncostatin M is a potential agent for the treatment of obesity and related metabolic disorders: a study in mice. *Diabetologia*, *58*(8), 1868-1876. https://doi.org/10.1007/s00125-015-3613-9

Komori, T., Tanaka, M., Senba, E., Miyajima, A., & Morikawa, Y. (2013). Lack of oncostatin M receptor beta leads to adipose tissue inflammation and insulin resistance by switching macrophage phenotype. *J Biol Chem*, *288*(30), 21861-21875. https://doi.org/10.1074/jbc.M113.461905

Lecker, S. H., Jagoe, R. T., Gilbert, A., Gomes, M., Baracos, V., Bailey, J., Price, S. R., Mitch, W. E., & Goldberg, A. L. (2004). Multiple types of skeletal muscle atrophy involve a common program of changes in gene expression. *FASEB J*, *18*(1), 39-51. https://doi.org/10.1096/fj.03-0610com

Lockhart, S. M., Saudek, V., & O'Rahilly, S. (2020). GDF15: A Hormone Conveying Somatic Distress to the Brain. *Endocr Rev*, *41*(4). https://doi.org/10.1210/endrev/bnaa007

Luan, H. H., Wang, A., Hilliard, B. K., Carvalho, F., Rosen, C. E., Ahasic, A. M., Herzog, E. L., Kang, I., Pisani, M. A., Yu, S., Zhang, C., Ring, A. M., Young, L. H., & Medzhitov, R. (2019). GDF15 Is an Inflammation-Induced Central Mediator of Tissue Tolerance. *Cell*, *178*(5), 1231-1244 e1211. https://doi.org/10.1016/j.cell.2019.07.033

Marceca, G. P., Londhe, P., & Calore, F. (2020). Management of Cancer Cachexia: Attempting to Develop New Pharmacological Agents for New Effective Therapeutic Options. *Front Oncol*, *10*, 298. https://doi.org/10.3389/fonc.2020.00298

Miki, Y., Morioka, T., Shioi, A., Fujimoto, K., Sakura, T., Uedono, H., Kakutani, Y., Ochi, A., Mori, K., Shoji, T., Emoto, M., & Inaba, M. (2019). Oncostatin M induces C2C12 myotube atrophy by modulating muscle differentiation and degradation. *Biochem Biophys Res Commun*, *516*(3), 951-956. https://doi.org/10.1016/j.bbrc.2019.06.143

Ozen, S. D., & Kir, S. (2024). Ectodysplasin A2 receptor signaling in skeletal muscle pathophysiology. *Trends Mol Med*, *30*(5), 471-483. https://doi.org/10.1016/j.molmed.2024.02.002

Patel, H. J., & Patel, B. M. (2017). TNF-alpha and cancer cachexia: Molecular insights and clinical implications. *Life Sci*, *170*, 56-63. https://doi.org/10.1016/j.lfs.2016.11.033

Patsalos, O., Dalton, B., Leppanen, J., Ibrahim, M. A. A., & Himmerich, H. (2020). Impact of TNF-alpha Inhibitors on Body Weight and BMI: A Systematic Review and Meta-Analysis. *Front Pharmacol*, *11*, 481. https://doi.org/10.3389/fphar.2020.00481

Queiroz, A. L., Dantas, E., Ramsamooj, S., Murthy, A., Ahmed, M., Zunica, E. R. M., Liang, R. J., Murphy, J., Holman, C. D., Bare, C. J., Ghahramani, G., Wu, Z., Cohen, D. E., Kirwan, J. P., Cantley, L. C., Axelrod, C. L., & Goncalves, M. D. (2022). Blocking ActRIIB and restoring appetite reverses cachexia and improves survival in mice with lung cancer. *Nat Commun*, *13*(1), 4633. https://doi.org/10.1038/s41467-022-32135-0

Richards, C. D. (2013). The enigmatic cytokine oncostatin m and roles in disease. *ISRN Inflamm*, *2013*, 512103. https://doi.org/10.1155/2013/512103

Sandri, M. (2013). Protein breakdown in muscle wasting: role of autophagy-lysosome and ubiquitin-proteasome. *Int J Biochem Cell Biol*, *45*(10), 2121-2129. https://doi.org/10.1016/j.biocel.2013.04.023

Shum, A. M., Fung, D. C., Corley, S. M., McGill, M. C., Bentley, N. L., Tan, T. C., Wilkins, M. R., & Polly, P. (2015). Cardiac and skeletal muscles show molecularly distinct responses to cancer cachexia. *Physiol Genomics*, *47*(12), 588-599. https://doi.org/10.1152/physiolgenomics.00128.2014

Silva, K. A., Dong, J., Dong, Y., Dong, Y., Schor, N., Tweardy, D. J., Zhang, L., & Mitch, W. E. (2015). Inhibition of Stat3 activation suppresses caspase-3 and the ubiquitin-proteasome system, leading to preservation of muscle mass in cancer cachexia. *J Biol Chem*, *290*(17), 11177-11187. https://doi.org/10.1074/jbc.M115.641514

Sofen, H., Bissonnette, R., Yosipovitch, G., Silverberg, J. I., Tyring, S., Loo, W. J., Zook, M., Lee, M., Zou, L., Jiang, G. L., & Paolini, J. F. (2023). Efficacy and safety of vixarelimab, a human monoclonal oncostatin M receptor beta antibody, in moderate-to-severe prurigo nodularis: a randomised, double-blind, placebo-controlled, phase 2a study. *EClinicalMedicine*, *57*, 101826. https://doi.org/10.1016/j.eclinm.2023.101826

Springer, M. L., Rando, T. A., & Blau, H. M. (2002). Gene delivery to muscle. *Curr Protoc Hum Genet*, *Chapter 13*, Unit13.14. https://doi.org/10.1002/0471142905.hg1304s31

Stross, C., Radtke, S., Clahsen, T., Gerlach, C., Volkmer-Engert, R., Schaper, F., Heinrich, P. C., & Hermanns, H. M. (2006). Oncostatin M receptor-mediated signal transduction is negatively regulated by SOCS3 through a receptor tyrosine-independent mechanism. *J Biol Chem*, *281*(13), 8458-8468. https://doi.org/10.1074/jbc.M511212200

Suriben, R., Chen, M., Higbee, J., Oeffinger, J., Ventura, R., Li, B., Mondal, K., Gao, Z., Ayupova, D., Taskar, P., Li, D., Starck, S. R., Chen, H. H., McEntee, M., Katewa, S. D., Phung, V., Wang, M., Kekatpure, A., Lakshminarasimhan, D., . . . Allan, B. B. (2020). Antibody-mediated inhibition of GDF15-GFRAL activity reverses cancer cachexia in mice. *Nat Med*, *26*(8), 1264-1270. https://doi.org/10.1038/s41591-020-0945-x

Tjondrokoesoemo, A., Schips, T., Kanisicak, O., Sargent, M. A., & Molkentin, J. D. (2016). Genetic overexpression of Serpina3n attenuates muscular dystrophy in mice. *Hum Mol Genet*, *25*(6), 1192-1202. https://doi.org/10.1093/hmg/ddw005

Urso, M. L., Chen, Y. W., Scrimgeour, A. G., Lee, P. C., Lee, K. F., & Clarkson, P. M. (2007). Alterations in mRNA expression and protein products following spinal cord injury in humans. *J Physiol*, *579*(Pt 3), 877-892. https://doi.org/10.1113/jphysiol.2006.118042

Urso, M. L., Scrimgeour, A. G., Chen, Y. W., Thompson, P. D., & Clarkson, P. M. (2006). Analysis of human skeletal muscle after 48 h immobilization reveals alterations in mRNA and protein for extracellular matrix components. *J Appl Physiol (1985)*, *101*(4), 1136-1148. https://doi.org/10.1152/japplphysiol.00180.2006

Voit, A., Patel, V., Pachon, R., Shah, V., Bakhutma, M., Kohlbrenner, E., McArdle, J. J., Dell'Italia, L. J., Mendell, J. R., Xie, L. H., Hajjar, R. J., Duan, D., Fraidenraich, D., & Babu, G. J. (2017). Reducing sarcolipin expression mitigates Duchenne muscular dystrophy and associated cardiomyopathy in mice. *Nat Commun*, *8*(1), 1068. https://doi.org/10.1038/s41467-017-01146-7

Wang, L. H., Friedman, S. D., Shaw, D., Snider, L., Wong, C. J., Budech, C. B., Poliachik, S. L., Gove, N. E., Lewis, L. M., Campbell, A. E., Lemmers, R., Maarel, S. M.,

Tapscott, S. J., & Tawil, R. N. (2019). MRI-informed muscle biopsies correlate MRI with pathology and DUX4 target gene expression in FSHD. *Hum Mol Genet*, *28*(3), 476-486. https://doi.org/10.1093/hmg/ddy364

Webster, J. M., Kempen, L., Hardy, R. S., & Langen, R. C. J. (2020). Inflammation and Skeletal Muscle Wasting During Cachexia. *Front Physiol*, *11*, 597675. https://doi.org/10.3389/fphys.2020.597675

West, N. R., Owens, B. M. J., & Hegazy, A. N. (2018). The oncostatin M-stromal cell axis in health and disease. *Scand J Immunol*, *88*(3), e12694. https://doi.org/10.1111/sji.12694

Wilkinson, D. J., Piasecki, M., & Atherton, P. J. (2018). The age-related loss of skeletal muscle mass and function: Measurement and physiology of muscle fibre atrophy and muscle fibre loss in humans. *Ageing Res Rev*, *47*, 123-132. https://doi.org/10.1016/j.arr.2018.07.005

Wolf, C. L., Pruett, C., Lighter, D., & Jorcyk, C. L. (2023). The clinical relevance of OSM in inflammatory diseases: a comprehensive review. *Front Immunol*, *14*, 1239732. https://doi.org/10.3389/fimmu.2023.1239732

Xiao, F., Wang, H., Fu, X., Li, Y., Ma, K., Sun, L., Gao, X., & Wu, Z. (2011). Oncostatin M inhibits myoblast differentiation and regulates muscle regeneration. *Cell Res*, *21*(2), 350-364. https://doi.org/10.1038/cr.2010.144

Xu, S., & Neamati, N. (2013). gp130: a promising drug target for

cancer therapy.

Yang, H., Mammen, J., Wei, W., Menconi, M., Evenson, A., Fareed, M., Petkova, V., & Hasselgren, P. O. (2005). Expression and activity of C/EBPbeta and delta are upregulated by dexamethasone in skeletal muscle. *J Cell Physiol*, *204*(1), 219-226. https://doi.org/10.1002/jcp.20278

Zarling J., S. M., MARQUARDT H.,,HANSON M.B.,LIOUBIN M.,TODARO GJ. (1986). OncostatinM: A growth regulator produced by differentiated histiocytic lymphoma cells.

Zhou, T., Wang, B., Liu, H., Yang, K., Thapa, S., Zhang, H., Li, L., & Yu, S. (2018). Development and validation of a clinically applicable score to classify cachexia stages in advanced cancer patients. *J Cachexia Sarcopenia Muscle*, *9*(2), 306-314. https://doi.org/10.1002/jcsm.12275